

# Surface Chern-Simons theory for third-order topological insulators and superconductors

Zhi-Hao Huang,<sup>1,2</sup> Yi Tan,<sup>1</sup> Wei Jia,<sup>3</sup> Long Zhang,<sup>4,2</sup> and Xiong-Jun Liu<sup>1,2,5,6,\*</sup>

<sup>1</sup>International Center for Quantum Materials and School of Physics, Peking University, Beijing 100871, China

<sup>2</sup>Hefei National Laboratory, Hefei 230088, China

<sup>3</sup>Key Laboratory of Quantum Theory and Applications of MoE, Lanzhou Center for Theoretical Physics, and Key Laboratory of Theoretical Physics of Gansu Province, Lanzhou University, Lanzhou 730000, China

<sup>4</sup>School of Physics and Institute for Quantum Science and Engineering, Huazhong University of Science and Technology, Wuhan 430074, China

<sup>5</sup>International Quantum Academy, Shenzhen 518048, China

<sup>6</sup>CAS Center for Excellence in Topological Quantum Computation, University of Chinese Academy of Sciences, Beijing 100190, China

Three-dimensional 3rd-order topological insulators (TOTIs) and superconductors (TOTSCs), as the highest-order topological phases hosting zero corner modes in physical dimension, has sparked extensive research interest. However, such topological states have not been discovered in reality due to the lack of experimental schemes of realization. Here, we propose a novel surface Chern-Simons (CS) theory for 3rd-order topological phases, and show that the theory enables a feasible and systematic design of TOTIs and TOTSCs. We show that the emergence of zero Dirac (Majorana) corner modes is entirely captured by an emergent  $\mathbb{Z}_2$  CS term that can be further characterized by a novel two-particle Wess-Zumino (WZ) term uncovered here in the surfaces of three-dimensional topological materials. Importantly, our proposed CS term characterization and two-particle WZ term mechanism provide a unique perspective to design TOTIs (TOTSCs) in terms of minimal ingredients, feasibly guiding the search for underlying materials, with promising candidates being discussed. This work shall advance both the theoretical and experimental research for highest-order topological matters.

**Introduction.**—Higher-order topological phases, an extension of conventional first-order topological phases [1–3], have recently gained significant attention [4–13]. Generally, the  $n^{\text{th}}$ -order topological insulators (TIs) or superconductors (TSCs) in  $d$  dimension ( $dD$ ) feature topologically protected gapless states on its  $(d - n)D$  boundary, but are gapped elsewhere. In order to classify and identify these exotic topological phases, various theoretical frameworks relying on detailed bulk properties have been developed, such as nested Wilson loop [4, 5], symmetry indicators [14, 15], magnetic topological quantum chemistry [16] and other approaches [17–20]. The higher-order topological phases are also intricately linked to broader research topics like non-Hermitian physics [21–23] and fracton orders [24].

Till now, there has been a significant focus on 2nd-order cases [25–48]. Specifically, the 2D 2nd-order TSCs have been extensively investigated [49–57] as Majorana corner modes exhibit non-Abelian statistics [58–64] which is pivotal for topological quantum computation [65, 66]. Moreover, the experimental schemes have also been proposed to generate 3D 2nd-order TIs (TSCs): applying Zeeman field [67], strain [8] and  $s$ -wave pairing [68] to 3D parent topological phases can induce gapless hinge modes. The materials, e.g. bismuth [69], WTe<sub>2</sub> [70] and FeSe [71] have been identified experimentally to support 3D 2nd-order TIs and TSCs, respectively. However, in contrast to 2nd-order topological phases, much less is known about 3rd-order topological insulators (TOTIs) and superconductors (TOTSCs) [72–80], and even less is achieved in experiment. Currently, two critical issues confront the third-order scenario and hinder the further development of this field. First, while the TOTIs and TOTSCs can be predicted by the classification theories [18–20, 72, 78], their 3rd-order zero corner mode lacks an intuitive and unified char-

acterization theories that benefit the realization. Second, the few existing proposals [73–75, 77, 80] for realizing TOTIs or TOTSCs are indeed short of physical feasibility and hard to achieve in experiment, incapable of providing efficient guidance in searching for underlying material candidates.

In this letter, we address the above critical issues and develop a novel surface Chern-Simons (CS) theory that is applicable generally to TOTIs and TOTSCs, and show that the theory enables a feasible and intuitive principle in search for real material candidates. We show that the presence of zero-energy corner modes in TOTIs and TOTSCs is dictated by a  $\mathbb{Z}_2$  CS term [81, 82], which is defined within a synthetic 3D space and relies on two winding numbers derived from surface mass fields and Dirac (or Majorana) cones. Further, we bring up an original two-particle Wess-Zumino (WZ) term in the surfaces of 3D TIs (TSCs), which also characterizes the Dirac and Majorana corner modes. The surface CS theory and two-particle WZ term provide new and intuitive characterization of the 3rd-order zero corner modes and, more importantly, inspire us to propose the realistic models of TOTI (TOTSC) based on 2D surface construction. In particular, applying staggered (or uniform) in-plane Zeeman fields and certain spin-orbit coupling (SOC) to conventional 3D TIs (TSCs) drives the systems into 3rd-order phases with Dirac (Majorana) zero corner modes. This facilitates to search for real materials, with promising candidates being identified.

**CS term characterization.** — We start with the CS theory which enables a unified characterization of the zero corner modes of TOTIs and TOTSCs. This theory is inspired by a previous conclusion [82] that Majorana zero modes at the vortex cores in 2D superconductors are generically protected by an emerging CS invariant  $(-1)^{\nu_3} = \sum_i n_i w_i$ , where  $w_i$  denotes the phase winding of superconducting order projected

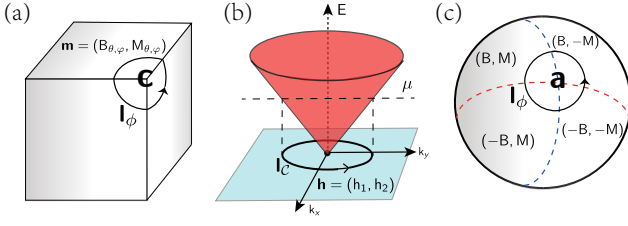


Figure 1. The CS characterization. (a) Illustration of the effective surface mass field  $\mathbf{m} = (B_{\theta,\varphi}, M_{\theta,\varphi})$ . Here, we employ a spherical coordinate frame with  $\theta(\varphi)$  denoting the polar (azimuth) angle.  $\mathcal{L}_\phi$  is a closed loop encircling the target corner  $\mathbf{c}$ . (b) Schematic of surface Dirac (Majorana) cone governed by  $\mathcal{H} = \mathbf{h}(\mathbf{k}) \cdot \Gamma$ , where the vector  $\mathbf{h} = (h_1, h_2)$  is a linear function of  $\mathbf{k}$  and  $\Gamma$  represents the gamma matrices. The loop  $\mathcal{L}_C$  is obtained by intersecting the Dirac (Majorana) cone with  $\mu = (B_\phi^2 + M_\phi^2)^{1/2}$ . (c) Mass field with  $\mathcal{W}_m = 1$ . We transform the cubic sample in (a) into a sphere without gap closing, so corner  $\mathbf{c}$  is mapped to  $\mathbf{a}$ , the intersection of two mass domain walls (red and blue dashed lines). Remarkably, a zero-energy bound state at  $\mathbf{a}$  corresponds to a zero corner mode at  $\mathbf{c}$ .

onto  $i$ -th FS and  $n_i$  is the integer vortex winding number (vorticity). A single Majorana zero mode is protected when the index  $\nu_3 = 1$ . For TOTIs and TOTSCs, it's important to highlight that the 3rd-order zero corner modes, which can be viewed as a unique type of defect-bound states, share similarities with vortex core modes. We then expect that the zero corner states may also be characterized by a similar CS term  $\tilde{\theta}$  resembling the framework of 2D theory.

Thereinafter, we derive the CS term  $\tilde{\theta}$  for the zero corner modes through an effective surface theory. The surface effective Hamiltonian of the TOTIs (TOTSCs) can be described generally as  $\mathcal{H}_{\text{surf}}^{\text{3rd}} = h_1(\mathbf{k})\Gamma_1 + h_2(\mathbf{k})\Gamma_2 + B_{\theta,\varphi}\Gamma_3 + M_{\theta,\varphi}\Gamma_4$  with  $\{\Gamma_i, \Gamma_j\} = 2\delta_{ij}$ , where  $\mathcal{H} = h_1(\mathbf{k})\Gamma_1 + h_2(\mathbf{k})\Gamma_2$  represents the effective Hamiltonian of surface Dirac (Majorana) cones and  $\mathbf{m} = (B_{\theta,\varphi}, M_{\theta,\varphi})$  constitutes the surface mass field [Fig.1(a)]. It is known that  $\tilde{\theta}$  can be defined on a manifold  $k^d \times \mathcal{M}^D$ , with  $d + D$  being odd [81]. To address this requirement, apart from 2D surface  $\mathbf{k}$ -space, we also focus on the loop  $\mathcal{L}_\phi$  [solid line in Fig.1(a)] surrounding target corner  $\mathbf{c}$  and take real space parameter  $\phi$  as a synthetic dimension of ring geometry  $\mathcal{S}^1$ . Then the surface Hamiltonian can be expressed in a compact 3D space  $k^3 = k^2 \times \mathcal{S}^1$  spanned by  $(\mathbf{k}, \phi)$  as follows:  $\mathcal{H}_{\text{surf}}^{\text{3rd}} = h_1(\mathbf{k})\Gamma_1 + h_2(\mathbf{k})\Gamma_2 + B_\phi\Gamma_3 + M_\phi\Gamma_4$ . And the Chern-Simons term is represented as  $\tilde{\theta} = \frac{1}{4\pi} \int d^3k \epsilon_{abc} \text{tr}[\mathcal{A}_a \partial_b \mathcal{A}_c + i_3^2 \mathcal{A}_a \mathcal{A}_b \mathcal{A}_c]$  where the non-Abelian Berry connection reads  $\mathcal{A}_{a=(\mathbf{k}, \phi)} = -i\langle \tilde{n} | \partial_a | \tilde{n}' \rangle$  and  $|\tilde{n}\rangle$  represents the degenerate eigenvector of occupied bands  $-E = -(h_1^2 + h_2^2 + B_\phi^2 + M_\phi^2)^{1/2}$ . We show that [83]

$$\tilde{\theta} = \pi \mathcal{W}_h \mathcal{W}_m, \quad (1)$$

where  $\mathcal{W}_h = \frac{1}{2\pi} \oint_{\mathcal{L}_C} d\mathbf{l} \cdot (h_2 \nabla_{\mathbf{k}} h_1 - h_1 \nabla_{\mathbf{k}} h_2) / (h_1^2 + h_2^2)$  and  $\mathcal{W}_m = \frac{1}{2\pi} \oint_{\mathcal{L}_\phi} d\phi (M_\phi \partial_\phi B_\phi - B_\phi \partial_\phi M_\phi) / (B_\phi^2 + M_\phi^2)$  represent the winding number for vector  $\mathbf{h} = (h_1, h_2)$  along contour  $\mathcal{L}_C$  [Fig.1(b)] and surface mass field  $\mathbf{m}$  on loop  $\mathcal{L}_\phi$ , respectively. If the surface Dirac (Majorana) cones dictated

by  $\mathcal{H} = h_1\Gamma_1 + h_2\Gamma_2$  contribute to  $\mathcal{W}_h = 1$ , as in usual TIs and TSCs, the CS term becomes  $\tilde{\theta} = \pi \mathcal{W}_m$ , indicating that  $\tilde{\theta}$  can be solely determined by the surface mass field.

We show that a nonzero  $\tilde{\theta}$  corresponds to a zero corner mode (see details in Supplementary Materials [83]). Fig.1(c) illustrates a nontrivial surface mass field, which exhibits a nonzero winding number  $\mathcal{W}_m = 1$ , and then  $\tilde{\theta} = \pi$ . In this case  $\mathcal{H}_{\text{surf}}^{\text{3rd}}$  resembles a 2D Dirac Hamiltonian with a vortex profile which binds a zero-energy bound state at the core, i.e. the target corner  $\mathbf{c}$ , indicating that it belongs to the symmetry class D [33, 81, 82]. Instead, no corner mode exists if the mass winding  $\mathcal{W}_m = 0$  [83]. Therefore, a nonzero  $\tilde{\theta} (\pm\pi)$  signifies the presence of zero corner mode of TOTIs or TOTSCs.

*Two-particle WZ term.*— A more intuitive characterization of the zero corner modes can be obtained by introducing an original topological invariant dubbed *Two-particle WZ term*, which is defined in the surfaces of the parent 3D TIs (TSCs). We show that the presence of zero corner modes can be contingent upon this term under specific conditions.

According to the “double-TI(TSC) construction” [14, 33, 34], we first stack two identical 3D time-reversal invariant TIs (TSCs) to construct a 3D total TIs (TSCs):  $\mathcal{H}_{\text{TI(TSC),total}}(\mathbf{k}) = \mathcal{H}_{\text{TI(TSC),\alpha}}(\mathbf{k}) \oplus \mathcal{H}_{\text{TI(TSC),\beta}}(\mathbf{k})$ , which yields two pairs of topological surface states  $\{|\varepsilon_{(1,2)}(\mathbf{r})\rangle\}_\alpha; \{|\varepsilon_{(3,4)}(\mathbf{r})\rangle\}_\beta$ . Here we can define the surface (pseudo)spin polarizations:  $\mathbf{n}_{\nu=(1,2,3,4)}(\mathbf{r}) = \langle \varepsilon_\nu(\mathbf{r}) | \mathbf{s} | \varepsilon_\nu(\mathbf{r}) \rangle$  [84–86], where Pauli matrix  $\mathbf{s}$  represents the spin degrees of freedom. Generally, (pseudo)spins are taken as the surface normal vector  $\mathbf{e}_r$  of 3D time-reversal invariant TIs (TSCs). We focus on an area  $\mathcal{S}$  of the surface of total TIs (TSCs), centered at corner  $\mathbf{c}$  [Fig.2(a)], and study the corresponding surface (pseudo)spin textures defined on it. As shown in Fig.2(b), a single  $\mathbf{n}_{\nu=(1,2,3,4)}$  within  $\mathcal{S}$  cannot form a complete sphere, but the joint textures of two polarizations  $\mathbf{n}_1$  and  $\mathbf{n}_2$  ( $\mathbf{1} = 1, 3; \mathbf{2} = 2, 4$ ) can constitute a “two-particle” unit sphere  $\bar{\mathcal{S}}_1 + \bar{\mathcal{S}}_2$  ( $\bar{\mathcal{S}}_3 + \bar{\mathcal{S}}_4$ ) in (pseudo)spin space under ideal condition, resembling a hedgehog ball. Thus we can define a novel *two-particle WZ term* on  $\mathcal{S}$ :

$$\tilde{n}_{\text{WZ}}^\alpha = \tilde{n}_{\text{WZ}}^\beta = \int_{\mathcal{S}} \frac{d\theta d\varphi}{2\pi} (\partial_\theta \tilde{\mathcal{A}}_\varphi - \partial_\varphi \tilde{\mathcal{A}}_\theta), \quad (2)$$

where  $\tilde{\mathcal{A}}_{\theta(\varphi)} = -i\langle \varepsilon_1 | \otimes \langle \varepsilon_2 | \partial_{\theta(\varphi)} | \varepsilon_1 \rangle \otimes | \varepsilon_2 \rangle$  represents two-particle Berry connection, with  $\theta(\varphi)$  being polar (azimuthal) angle in real space. As displayed in Fig.2(c), we find that Eq.(2) can further reduce to a winding number of the normal vector  $\mathbf{e}_{\tilde{r}}$  along the equator of unit sphere  $\bar{\mathcal{S}}_1 + \bar{\mathcal{S}}_2$  ( $\bar{\mathcal{S}}_3 + \bar{\mathcal{S}}_4$ ):  $\tilde{n}_{\text{WZ}}^\alpha = \tilde{n}_{\text{WZ}}^\beta = \oint_{\text{equator}} \frac{d\varphi}{2\pi} [\mathbf{e}_{\tilde{z}} \cdot (\mathbf{e}_{\tilde{r}}|_{\tilde{\theta}=\frac{\pi}{2}} \times \partial_{\tilde{\varphi}} \mathbf{e}_{\tilde{r}}|_{\tilde{\theta}=\frac{\pi}{2}})]$ , where  $\tilde{\theta}(\tilde{\varphi})$  denotes the polar (azimuthal) angle in (pseudo)spin space with respect to base vector  $\mathbf{e}_{\tilde{z}}$  which is chosen as the vector  $\mathbf{e}_{r=r_c}$  from “center of  $\partial\mathcal{S}$ ” [83] to corner  $\mathbf{c}$ . Notice that  $\tilde{n}_{\text{WZ}}$  is an intuitive topological invariant that emerges from (pseudo)spin textures around target corner and contains the necessary surface information used for identifying the corner modes of TOTIs and TOTSCs.

We then apply a certain surface mass field  $\mathbf{m} = (\mathbf{e}_r \cdot \mathbf{B}, \mathbf{e}_r \cdot \mathbf{M})$  ( $\mathbf{B}$  and  $\mathbf{M}$  are constant unit vectors with  $\mathbf{M} \times \mathbf{B} \neq 0$ )

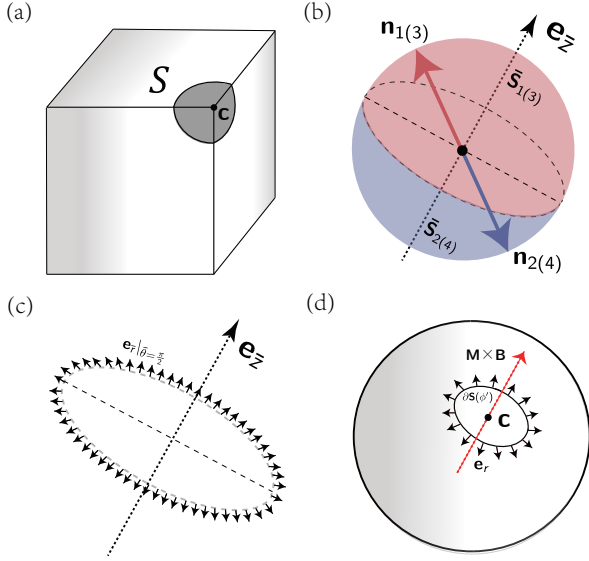


Figure 2. The two-particle WZ mechanism. (a) Area  $S$  centered at the target corner  $c$ . (b) (Pseudo)spin textures within  $S$  in (pseudo)spin space. Due to the “double-TI(TSC) construction”, we define two pairs of (pseudo)spin polarizations  $\{\mathbf{n}_1, \mathbf{n}_2\}$  and  $\{\mathbf{n}_3, \mathbf{n}_4\}$  with  $\mathbf{n}_1 = -\mathbf{n}_2 = \mathbf{n}_3 = -\mathbf{n}_4 = \mathbf{e}_r$ . Ideally, each group of (pseudo)spins form perfect unit spherical surfaces  $\tilde{S}_{1(3)} + \tilde{S}_{2(4)}$  in (pseudo)spin space, and the total (pseudo)spin textures coincide. Note that the vector  $\mathbf{e}_{r=r_c}$  is required to be the  $\mathbf{e}_z$  in (pseudo)spin space. (c) The winding of  $\mathbf{e}_{r|\bar{\theta}=\frac{\pi}{2}}$  along the equator of  $\tilde{S}_{1(3)} + \tilde{S}_{2(4)}$ . (d) The winding of  $\mathbf{e}_r$  on the boundary  $\partial S$  encircling the corner  $c$ . The vector  $\mathbf{M} \times \mathbf{B}$  is parallel to  $\mathbf{e}_{r=r_c}$ .

to gap out the surface of total TIs (TSCs) to achieve the TOTIs (TOTSCs). The CS term about corner  $c$  reads  $\tilde{\theta} = \oint_{\partial S(\phi')} \frac{d\phi'}{2} |\mathbf{M} \times \mathbf{B}| [e_{\mathbf{M} \times \mathbf{B}} \cdot (\mathbf{e}_r \times \partial_{\phi'} \mathbf{e}_r)] / [(e_r \cdot \mathbf{B})^2 + (e_r \cdot \mathbf{B})^2]$ , which is also related to the winding of  $\mathbf{e}_r$  [Fig.2(d)].

Combining the  $\tilde{n}_{\text{WZ}}$  and  $\tilde{\theta}$  derived above, we reach that [83]

$$|\tilde{\theta}| = \pi |\tilde{n}_{\text{WZ}}^\alpha| = \pi |\tilde{n}_{\text{WZ}}^\beta|, \quad (3)$$

which is a key result that the two-particle WZ term leads to a non-zero CS term in the presence of the mass field  $(\mathbf{e}_r \cdot \mathbf{B}, \mathbf{e}_r \cdot \mathbf{M})$ . Thus, if the surface (pseudo)spin textures around the target corner has a nonzero two-particle WZ term ( $\tilde{n}_{\text{WZ}}^\alpha = \tilde{n}_{\text{WZ}}^\beta = 1$ ), a topological zero corner mode emerges whenever the mass field  $(\mathbf{e}_r \cdot \mathbf{B}, \mathbf{e}_r \cdot \mathbf{M})$  is introduced. We note that the (pseudo)spin textures within  $S$  may not constitute a perfect unit spherical surface, but can be connected to a unit spherical surface through the “continuation” which does not bring about additional nodes of mass. A non-zero  $\tilde{n}_{\text{WZ}}$  is obtained as long as the actual surface (pseudo)spin textures cover the area where the mass nodes are obtained [83].

Before proceeding, we clarify two points about the surface Chern-Simons theory. (I) The characterization theory based on  $\tilde{\theta}$  is built on the general effective surface Hamiltonian rather than detailed bulk properties [18–20, 72, 78], making it applicable to generic TOTIs and TOTSCs, irrespective of the concrete methods for achieving these phases. (II) The  $\tilde{n}_{\text{WZ}}$

mechanism shows a rather intuitive physical characterization: the corner modes are associated with the surface (pseudo)spin textures that are governed by the mass field. These features provide a powerful guidance in constructing the physical models and facilitate the search for real materials.

*Physical realizations.*— The surface Chern-Simons theory offers a unique perspective for the emergence of zero corner modes—it opens new pathways to develop realistic physical models for TOTIs (TOTSCs) via the mass field construction. In the following, we shall introduce implementation strategies for TOTSCs and TOTIs in terms of  $\tilde{\theta}$  characterization and  $\tilde{n}_{\text{WZ}}$  mechanism, respectively, with which the promising candidates will be discussed. Now let us begin with

$$\mathcal{H}_{\text{TOTSC}}(\mathbf{k}) = \mathcal{H}_{\text{TSC}}^{\text{total}}(\mathbf{k}) + \mathbf{B}_{\parallel} \cdot \mathbf{s} + \lambda_{so}(\mathbf{k}) \sigma_y s_z, \quad (4)$$

where  $\lambda_{so}(\mathbf{k}) = \lambda_{so,0} - \lambda_{so,1}(\cos k_x + \cos k_y)$ . The total TSC comprises two copies of TSCs ( $\mathcal{H}_{\text{TSC},\alpha} \oplus \mathcal{H}_{\text{TSC},\beta}$ ) with the same winding numbers [81] and the Hamiltonian is given by  $\mathcal{H}_{\text{TSC},\text{total}}(\mathbf{k}) = (\Delta_p/k_F) \sum_{j=x,y} \sin k_j \sigma_0 \tau_x s_j + (\Delta_p/k_F) \sin k_z \sigma_z \tau_x s_z - [\mu - 3/m_* + (1/m_*) \sum_{j=x,y,z} \cos k_j] \sigma_z \tau_z s_0$ . Here,  $\sigma$ ,  $\tau$  and  $s$  denote the orbital, Nambu and spin degrees of freedom, respectively. As shown in Fig.3(a), two orbitals ( $\alpha, \beta$ ) are depicted at each site. The mass field is given by the last two terms of Eq.(4), namely, the Zeeman term originated from an in-plane magnetic field  $\mathbf{B}_{\parallel} = (1/\sqrt{2})(\mathbf{e}_x + \mathbf{e}_y)$  and the SOC term preserving time-reversal symmetry:  $\hat{T}^{-1} \lambda_{so}(\mathbf{k}) \sigma_y s_z \hat{T} = \lambda_{so}(-\mathbf{k}) \sigma_y s_z$ . Note that the SOC term, involving the real-space on-site and nearest-neighbour parts shown in Fig.3(b), is captured by  $\hat{H}_{\text{SOC}}^I = \sum_i -i \lambda_{so,0} (\hat{c}_{i,\alpha}^\dagger s_z \hat{c}_{i,\beta} - \hat{c}_{i,\beta}^\dagger s_z \hat{c}_{i,\alpha}) + \sum_{\langle i,j \rangle} (\frac{i \lambda_{so,1}}{2} \hat{c}_{i,\alpha}^\dagger s_z \hat{c}_{j,\beta} + \text{h.c.})$  [87, 88], where  $\lambda_{so,0}$  and  $\lambda_{so,1}$  represent the corresponding SOC strengths.

Using the  $\tilde{\theta}$  characterization, we can predict Majorana zero corner modes. The surface effective mass field is given by  $\mathbf{m} = (m_\phi, m_\theta)$  [83]. Here  $m_\phi$  is induced by the magnetic field that is confined to the  $x - y$  plane, and the mass domain wall of  $m_\phi$  spreads along one meridian  $\mathbf{l}_\phi$ . Meanwhile,  $m_\theta$  induced by  $\mathcal{H}_{\text{SOC}}(\mathbf{k})$  creates two additional domain walls at parallels  $\mathbf{l}_{\theta_1}$  and  $\mathbf{l}_{\theta_2}$ . The intersections of  $\mathbf{l}_\phi$  and  $\mathbf{l}_{\theta_{1(2)}}$  in Fig.3(c) represent mass field vortex cores with  $\mathcal{W}_m = 1$ . Thus the TOTSC hosts four Majorana zero corner modes. Numerical results shown in Fig.3(d) support this prediction.

The proposal for TOTIs follows a similar approach. We consider the Hamiltonian

$$\mathcal{H}_{\text{TOTI}}(\mathbf{k}) = \mathcal{H}_{\text{TI}}^{\text{total}}(\mathbf{k}) + \rho_z \mathbf{B}_{\parallel} \cdot \mathbf{s} + \rho_y \mathbf{M} \cdot \mathbf{s}, \quad (5)$$

where the total TI Hamiltonian reads  $\mathcal{H}_{\text{TI}}^{\text{total}}(\mathbf{k}) = \mathcal{H}_{\text{TI}}^a(\mathbf{k}) \oplus \mathcal{H}_{\text{TI}}^b(\mathbf{k}) = (m - t \sum_i \cos k_i) \rho_0 s_0 \sigma_z + t (\sum_i \sin k_i \rho_0 s_i) \sigma_x$ , and  $\rho$  denotes the Pauli matrix for sublattice degrees of freedom. We explore the constant terms  $(\rho_z \mathbf{B}_{\parallel} \cdot \mathbf{s}, \rho_y \mathbf{M} \cdot \mathbf{s})$  with  $\mathbf{B}_{\parallel} = -B \mathbf{e}_y$  and  $\mathbf{M} = \lambda_{so} \mathbf{e}_z$ . The staggered Zeeman term  $\rho_z \mathbf{B}_{\parallel} \cdot \mathbf{s}$  can be implemented by applying anti-ferromagnetism between layers  $\{a\}$  and  $\{b\}$  as plotted in

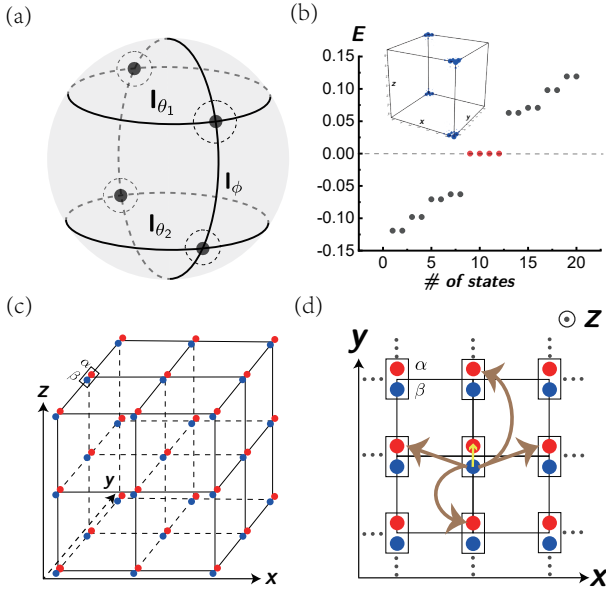


Figure 3. The TOTSC model is described by  $\tilde{\theta}$  characterization with parameters  $\mu = 2$ ,  $m_* = 0.5$ ,  $\Delta_p/k_F = 1$ ,  $\lambda_{so,0} = 1$ ,  $\lambda_{so,1} = 0.8$ , and  $|\mathbf{B}_{\parallel}| = 1$ . (a) The designed square lattice for this physical TOTSC model features  $\alpha$  and  $\beta$  orbitals within a unit cell, represented by red and blue dots, respectively. (b) The schematic illustration of  $\mathcal{T}$ -invariant spin-orbit coupling in real space, comprising on-site (yellow arrow) and nearest-neighbouring (brown arrow) terms. (c) Predicted distribution of surface effective mass field vortices by  $\tilde{\theta}$  characterization.  $\mathbf{l}_{\phi}$  and  $\mathbf{l}_{\theta_{1(2)}}$  represent mass domain walls resulting from the Zeeman and SOC terms, respectively. (d) Numerical results concerning TOTSCs, showing consistent numbers and positions of Majorana zero corner modes with theoretical predictions from Chern-Simons term  $\tilde{\theta}$  characterization.

Fig.4(a), while the  $\hat{\mathcal{T}}$ -invariant SOC shown in Fig.4(b) only remains the intra-unit cell term in the real space:  $\hat{H}_{\text{SOC}}^{\text{II}} = \sum_i -i\lambda_{so}(\hat{c}_{i,a}^\dagger s_z \hat{c}_{i,b} - \hat{c}_{i,b}^\dagger s_z \hat{c}_{i,a})$ . Here  $a$  and  $b$  denote different sublattice sites within a unit cell.

Remarkably, the two constant terms ( $\rho_z \mathbf{B}_{\parallel} \cdot \mathbf{s}$ ,  $\rho_y \mathbf{M} \cdot \mathbf{s}$ ) generate the desired surface mass field ( $\mathbf{e}_r \cdot \mathbf{B}_{\parallel}, \mathbf{e}_r \cdot \mathbf{M}$ ), and give rise to the corner modes of the TOTI according to the  $\tilde{n}_{\text{WZ}}$  mechanism. As illustrated in Fig.4(c), the (pseudo)spin textures around  $\mathbf{c}$  are actually not closed. However, we can find that the well-defined two-particle WZ term ( $\tilde{n}_{\text{WZ}}^a = \tilde{n}_{\text{WZ}}^b = 1$ ) is obtained by “continuation” as  $\mathbf{e}_{\mathbf{M} \times \mathbf{B}_{\parallel}} \parallel \mathbf{e}_x$  which does not involve mass nodes [83]. In consequence, a zero corner mode is obtained at the corner  $\mathbf{c}$ . The numerical results in Fig.4(d) confirm this analysis.

With the above physical schemes we can now propose the promising candidates for realization. In order to achieve the TOTSCs described by Eq.(4), besides the applied Zeeman field in the  $x - y$  plane, there should be at least two different orbitals ( $\alpha, \beta$ ) for each lattice site, with which the  $\hat{H}_{\text{SOC}}^{\text{I}}$  can be implemented. For our purpose the typical orbitals ( $\alpha, \beta$ ) can be  $(p_x, p_y)$ ,  $(d_{xz}, d_{yz})$ ,  $(d_{xy}, d_{x^2-y^2})$ . We then find a promising candidate based on the superconducting material  $\beta$ -PdBi<sub>2</sub> [89] which exhibits  $p$ -wave pairing [90, 91]

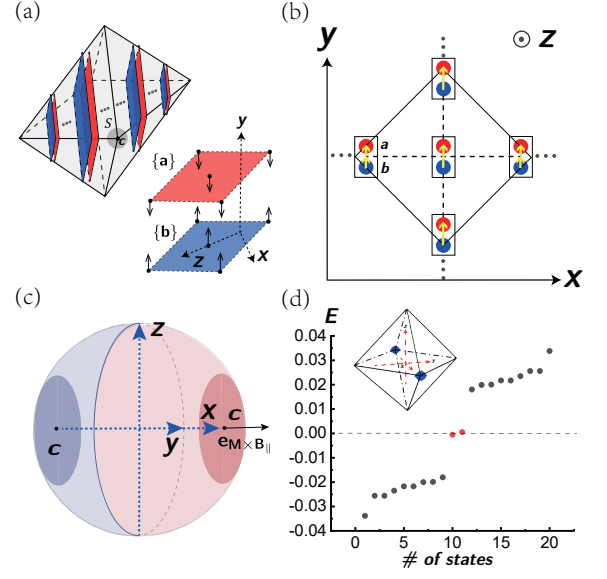


Figure 4. The  $\tilde{n}_{\text{WZ}}$  mechanism is applied to the physical model of TOTIs with parameters  $m = 2$ ,  $t = 1$ ,  $\lambda_{so} = 1$ , and  $\mathbf{B} = 1$ . (a) Sample geometry illustration:  $a$  and  $b$  represent different sublattice sites within a unit cell, and the corresponding layers  $\{a\}$  and  $\{b\}$  are alternately arranged. Antiferromagnetism can be induced between  $\{a\}$  and  $\{b\}$ . (b) Visualization of an alternative time-reversal invariant SOC in real space, featuring only the intra-cell term (yellow arrow) remaining. (c) (Pseudo)spin textures (deep red and deep blue regions) around the target corner  $\mathbf{c}$ . Although perfect spherical surfaces cannot be obtained from these textures, the  $\tilde{n}_{\text{WZ}}$  is still well-defined through “continuation” (light red and light blue regions denote auxiliary textures) due to  $\mathbf{e}_{\mathbf{M} \times \mathbf{B}_{\parallel}} = \mathbf{e}_{r=r_c}$ . (d) Numerical results validate the theoretical predictions.

and its topological surface states [92] meets the condition as the Fermi surface is mostly contributed from Bi ( $6p_x, 6p_y$ ) orbitals [93]. Thus the TOTSC could be realized by applying Zeeman field. As for the TOTIs in Eq.(5), there are also two key ingredients, the staggered Zeeman term  $\rho_z \mathbf{B}_{\parallel} \cdot \mathbf{s}$  and  $\hat{H}_{\text{SOC}}^{\text{II}}$ , in reaching this topological phase. Notably, the 3D antiferromagnetic (AFM) TI [94] can be an ideal platform to implement these terms since the staggered Zeeman field are naturally captured by the interlayer antiferromagnetism orders and the  $\hat{H}_{\text{SOC}}^{\text{II}}$  is very promising to be realized by inducing the spin-dependent couplings between neighbouring AFM layers. With this we conjecture that in the 3D AFM topological materials (e.g. MnBi<sub>2</sub>Te<sub>4</sub> [95–97]) introducing the spin-dependent interlayer couplings should generate the desired TOTI phases [83]. We note that while to further confirm the proposed candidates with more concrete details necessitates more sophisticated numerical methods [98, 99], our present theory has provided clear guidance in search for the 3rd-order TIs and TSCs in real materials.

**Conclusion.**— We have proposed the surface Chern-Simons theory for TOTIs and TOTSCs, which provides a unified and intuitive characterization of the Dirac and Majorana corner modes, and facilitates the physical realizations of these

3rd order zero modes. We showed that the CS term, dictating the existence of zero corner modes in all TOTIs and TOTSCs, is connected to mass field and Dirac (Majorana) cone winding numbers, and further to a novel two-particle WZ term derived from surface (pseudo)spin textures of the parent 3D topological materials. This intuitive topological characterization offers a fresh approach for realizing physical models of TOTIs (TOTSCs) and aid the search for real materials, of which the promising candidates have been discussed. This study opens up a clear route to discover 3rd-order topological matter in both theory and experiment.

*Acknowledgments.*— We thank Xin-Chi Zhou, Ting-Fung Jeffrey Poon, and Bao-Zong Wang for valuable discussions. This work was supported by National Key Research and Development Program of China (No. 2021YFA1400900), the National Natural Science Foundation of China (Grants No. 12261160368, No. 11825401, No. 12104205, and No. 11921005), and the Innovation Program for Quantum Science and Technology (Grant No. 2021ZD0302000).

---

\* Corresponding author: xiongjunliu@pku.edu.cn.

- [1] M. Z. Hasan, and C. L. Kane, Colloquium: Topological insulators, *Rev. Mod. Phys.* **82**, 3045 (2010).
- [2] X.-L. Qi, and S.-C. Zhang, Topological insulators and superconductors, *Rev. Mod. Phys.* **83**, 1057 (2011).
- [3] A. Bansil, H. Lin, and T. Das, Colloquium: Topological band theory, *Rev. Mod. Phys.* **88**, 021004 (2016).
- [4] W. A. Benalcazar, B. A. Bernevig, and T. L. Hughes, Quantized electric multipole insulators, *Science* **357**, 61 (2017).
- [5] W. A. Benalcazar, B. A. Bernevig, and T. L. Hughes, Electric multipole moments, topological multipole moment pumping, and chiral hinge states in crystalline insulators, *Phys. Rev. B* **96**, 245115 (2017).
- [6] J. Langbehn, Y. Peng, L. Trifunovic, F. von Oppen, and P. W. Brouwer, Reflection-symmetric second-order topological insulators and superconductors, *Phys. Rev. Lett.* **119**, 246401 (2017).
- [7] Z. Song, Z. Fang, and C. Fang,  $(d-2)$ -Dimensional Edge States of Rotation Symmetry Protected Topological States, *Phys. Rev. Lett.* **119**, 246402 (2017).
- [8] F. Schindler, A. M. Cook, M. G. Vergniory, Z. Wang, S. S. P. Parkin, B. A. Bernevig, and T. Neupert, Higher-order topological insulators, *Sci. Adv.* **4** (2018).
- [9] M. Geier, L. Trifunovic, M. Hoskam, and P. W. Brouwer, Second-order topological insulators and superconductors with an order-two crystalline symmetry, *Phys. Rev. B* **97**, 205135 (2018).
- [10] G. van Miert, and C. Ortix, Higher-order topological insulators protected by inversion and rotoinversion symmetries, *Phys. Rev. B* **98**, 081110(R) (2018).
- [11] M. Ezawa, Minimal models for Wannier-type higher-order topological insulators and phosphorene, *Phys. Rev. B* **98**, 045125 (2018).
- [12] D. Călugăru, V. Juričić, and B. Roy, Higher-order topological phases: A general principle of construction, *Phys. Rev. B* **99**, 041301 (2019).
- [13] F. Schindler, Dirac equation perspective on higher-order topological insulators, *Journal of Applied Physics* **128**, 221102 (2020).
- [14] E. Khalaf, H. C. Po, A. Vishwanath, and H. Watanabe, Symmetry Indicators and Anomalous Surface States of Topological Crystalline Insulators, *Phys. Rev. X* **8**, 031070 (2018).
- [15] F. Tang, H. C. Po, A. Vishwanath, and X. Wan, Efficient topological materials discovery using symmetry indicators, *Nat. Phys.* **15**, 470 (2019).
- [16] L. Elcoro, B. J. Wieder, Z. Song, Y. Xu, B. Bradlyn, and B. A. Bernevig, Magnetic topological quantum chemistry, *Nat Commun* **12**, 5965 (2021).
- [17] W. A. Benalcazar, T. Li, and T. L. Hughes, Quantization of fractional corner charge in  $C_n$ -symmetric higher-order topological crystalline insulators, *Phys. Rev. B* **99**, 245151 (2019).
- [18] L. Li, W. Zhu, and J. Gong, Direct dynamical characterization of higher-order topological phases with nested band inversion surfaces, *Sci. Bull.* **66**, 1502 (2021).
- [19] Z. Lei, Y. Deng, and L. Li, Topological classification of higher-order topological phases with nested band inversion surfaces, *Phys. Rev. B* **106**, 245105 (2022).
- [20] W. Jia, X.-C. Zhou, L. Zhang, L. Zhang, X.-J. Liu, Unified characterization for higher-order topological phase transitions, *Phys. Rev. Research* **5**, L022032 (2023).
- [21] K. Kawabata, M. Sato, and K. Shiozaki, Higher-order non-Hermitian skin effect, *Phys. Rev. B* **102**, 205118 (2020).
- [22] R. Okugawa, R. Takahashi, and K. Yokomizo, Second-order topological non-Hermitian skin effects, *Phys. Rev. B* **102**, 241202 (2020).
- [23] D. Zou, T. Chen, W. He, J. Bao, C. H. Lee, H. Sun, and X. Zhang, Observation of hybrid higher-order skin-topological effect in non-Hermitian topoelectrical circuits, *Nat Commun* **12**, 7201 (2021).
- [24] Y. You, F. J. Burnell, and T. L. Hughes, Multipolar topological field theories: Bridging higher order topological insulators and fractons, *Phys. Rev. B* **103**, 245128 (2021).
- [25] X.-L. Sheng, C. Chen, H. Liu, Z. Chen, Z.-M. Yu, Y. X. Zhao, and S. A. Yang, Two-Dimensional Second-Order Topological Insulator in Graphdiyne, *Phys. Rev. Lett.* **123**, 256402 (2019).
- [26] B. Liu, G. Zhao, Z. Liu, and Z. F. Wang, Two-Dimensional Quadrupole Topological Insulator in  $\gamma$ -Graphyne, *Nano Lett.* **19**, 6492 (2019).
- [27] E. Lee, R. Kim, J. Ahn, and B.-J. Yang, Two-dimensional higher-order topology in monolayer graphdiyne, *npj Quantum Mater.* **5**, 1 (2020).
- [28] Y. Ren, Z. Qiao, and Q. Niu, Engineering Corner States from Two-Dimensional Topological Insulators, *Phys. Rev. Lett.* **124**, 166804 (2020).
- [29] C. Chen, Z. Song, J.-Z. Zhao, Z. Chen, Z.-M. Yu, X.-L. Sheng, and S. A. Yang, Universal Approach to Magnetic Second-Order Topological Insulator, *Phys. Rev. Lett.* **125**, 056402 (2020).
- [30] C. Chen, W. Wu, Z.-M. Yu, Z. Chen, Y. X. Zhao, X.-L. Sheng, and S. A. Yang, Graphyne as a second-order and real Chern topological insulator in two dimensions, *Phys. Rev. B* **104**, 085205 (2021).
- [31] F. Liu, and K. Wakabayashi, Higher-order topology and fractional charge in monolayer graphene, *Phys. Rev. Research* **3**, 023121 (2021).
- [32] B. Liu, L. Xian, H. Mu, G. Zhao, Z. Liu, A. Rubio, and Z. F. Wang, Higher-Order Band Topology in Twisted Moiré Superlattice, *Phys. Rev. Lett.* **126**, 066401 (2021).
- [33] E. Khalaf, Higher-order topological insulators and superconductors protected by inversion symmetry, *Phys. Rev. B* **97**, 205136 (2018).
- [34] N. Bultinck, B. A. Bernevig, and M. P. Zaletel, Three-dimensional superconductors with hybrid higher-order topology, *Phys. Rev. B* **99**, 125149 (2019).
- [35] A. Matsugatani, and H. Watanabe, Connecting higher-order

- topological insulators to lower-dimensional topological insulators, *Phys. Rev. B* **98**, 205129 (2019).
- [36] Y. Peng, and Y. Xu, Proximity-induced Majorana hinge modes in antiferromagnetic topological insulators, *Phys. Rev. B* **99**, 195431 (2019).
- [37] Y. Xu, Z. Song, Z. Wang, H. Weng, and X. Dai, Higher-Order Topology of the Axion Insulator  $\text{EuIn}_2\text{As}_2$ , *Phys. Rev. Lett.* **122**, 256402 (2019).
- [38] Y. Peng, and G. Refael, Floquet second-order topological insulators from nonsymmorphic space-time symmetries, *Phys. Rev. Lett.* **123**, 016806 (2019).
- [39] R. Queiroz, and A. Stern, Splitting the hinge mode of higher-order topological insulators, *Phys. Rev. Lett.* **123**, 036802 (2019).
- [40] Z. Yan, Higher-order topological odd-parity superconductors, *Phys. Rev. Lett.* **123**, 177001 (2019).
- [41] A. Skurativska, T. Neupert, and M. H. Fischer, Atomic limit and inversion-symmetry indicators for topological superconductors, *Rev. Research* **2**, 013064 (2020).
- [42] H. Li, and K. Sun, Pfaffian formalism for higher-order topological insulators, *Phys. Rev. Lett.* **124**, 036401 (2020).
- [43] K. Plekhanov, F. Ronetti, D. Loss, and J. Klinovaja, Hinge states in a system of coupled Rashba layers, *Phys. Rev. Research* **2**, 013083 (2020).
- [44] R. Takahashi, Y. Tanaka, and S. Murakami, Bulk-edge and bulk-hinge correspondence in inversion-symmetric insulators, *Phys. Rev. Research* **2**, 013300 (2020).
- [45] R.-X. Zhang, F. Wu, and S. D. Sarma, Mi $\ddot{u}$ ebius Insulator and Higher-Order Topology in  $\text{MnBi}_{2n}\text{Te}_{3+1}$ , *Phys. Rev. Lett.* **124**, 136407 (2020).
- [46] C. Yoon, C.-C. Liu, H. Min, and F. Zhang, Quasi-One-Dimensional Higher-Order Topological Insulators, arXiv: 2005.14710.
- [47] X.-J. Luo, X.-H. Pan, and X. Liu, Higher-order topological superconductors based on weak topological insulators, *Phys. Rev. B* **104**, 104510 (2021).
- [48] N. M. Nguyen, W. Brzezicki, and T. Hyart, Corner states, hinge states, and Majorana modes in  $\text{SnTe}$  nanowires, *Phys. Rev. B* **105**, 075310 (2022).
- [49] T. Liu, J. J. He, and F. Nori, Majorana corner states in a two-dimensional magnetic topological insulator on a high-temperature superconductor, *Phys. Rev. B* **98**, 245413 (2018).
- [50] Q. Wang, C.-C. Liu, Y.-M. Lu, and F. Zhang, High-Temperature Majorana Corner States, *Phys. Rev. Lett.* **121**, 186801 (2018).
- [51] Z. Yan, F. Song, and Z. Wang, Majorana Corner Modes in a High-Temperature Platform, *Phys. Rev. Lett.* **121**, 096803 (2018).
- [52] Z. Yan, Higher-order topological odd-parity superconductors, *Phys. Rev. Lett.* **123**, 177001 (2019).
- [53] X. Zhu, Second-order topological superconductors with mixed pairing, *Phys. Rev. Lett.* **122**, 236401 (2019).
- [54] Y. Volpez, D. Loss, and J. Klinovaja, Second-Order Topological Superconductivity in  $\pi$ -Junction Rashba Layers, *Phys. Rev. Lett.* **122**, 126402 (2019).
- [55] C. Zeng, T. D. Stanescu, C. Zhang, V. W. Scarola, and S. Tewari, Majorana Corner Modes with Solitons in an Attractive Hubbard-Hofstadter Model of Cold Atom Optical Lattices, *Phys. Rev. Lett.* **123**, 060402 (2019).
- [56] X.-H. Pan, K.-J. Yang, L. Chen, G. Xu, C.-X. Liu, and X. Liu, Lattice-Symmetry-Assisted Second-Order Topological Superconductors and Majorana Patterns, *Phys. Rev. Lett.* **123**, 156801 (2019).
- [57] R.-X. Zhang, W. S. Cole, X. Wu, and S. Das Sarma, Higher-Order Topology and Nodal Topological Superconductivity in  $\text{Fe}(\text{Se},\text{Te})$  Heterostructures, *Phys. Rev. Lett.* **123**, 167001 (2019).
- [58] C. Nayak and F. Wilczek,  $2n$ -quasihole states realize  $2^n-1$ -dimensional spinor braiding statistics in paired quantum Hall states, *Nucl. Phys. B* **3**, 529 (1996).
- [59] D. A. Ivanov, Non-Abelian Statistics of Half-Quantum Vortices in  $p$ -Wave Superconductors, *Phys. Rev. Lett.* **86**, 268 (2001).
- [60] S. Das Sarma, M. Freedman, and C. Nayak, Topologically Protected Qubits from a Possible Non-Abelian Fractional Quantum Hall State, *Phys. Rev. Lett.* **94**, 166802 (2005).
- [61] J. Alicea, Y. Oreg, G. Refael, F. Von Oppen, and M. P. Fisher, Non-Abelian statistics and topological quantum information processing in 1D wire networks, *Nat. Phys.* **7**, 412 (2011).
- [62] X.-J. Liu, C. L. M. Wong, and K. T. Law, Non-abelian majorana doublets in time-reversal-invariant topological superconductors, *Phys. Rev. X* **4**, 021018 (2014).
- [63] P. Gao, Y.-P. He, and X.-J. Liu, Symmetry-protected non-Abelian braiding of Majorana Kramers pairs, *Phys. Rev. B* **94**, 224509 (2016); **95**, 019902(E) (2017).
- [64] J.-S. Hong, T.-F. J. Poon, L. Zhang, and X.-J. Liu, Unitary symmetry-protected non-Abelian statistics of Majorana modes, *Phys. Rev. B* **105**, 024503 (2022).
- [65] R.W. Bomantara, and J. Gong, Measurement-only quantum computation with Floquet Majorana corner modes, *Phys. Rev. B* **101**, 085401 (2020).
- [66] T. E. Pahomi, M. Sigrist, and A. A. Soluyanov, Braiding Majorana corner modes in a second-order topological superconductor, *Phys. Rev. Research* **2**, 032068(R) (2020).
- [67] Y.-J. Wu, J. Hou, Y.-M. Li, X.-W. Luo, X. Shi, and C. Zhang, In-Plane Zeeman-Field-Induced Majorana Corner and Hinge Modes in an  $s$ -Wave Superconductor Heterostructure, *Phys. Rev. Lett.* **124**, 227001 (2020).
- [68] R.-X. Zhang, W. S. Cole, and S. D. Sarma, Helical Hinge Majorana Modes in Iron-Based Superconductors, *Phys. Rev. Lett.* **122**, 187001 (2019).
- [69] F. Schindler, Z. Wang, B. A. Bernevig, and T. Neupert, Higher-order topology in bismuth, *Nat. Phys.* **14**, 918 (2018).
- [70] M. H. Jo, and H. Choi, Spinful hinge states in the higher-order topological insulators  $\text{WTe}_2$ , *Nat Commun* **14**, 1801 (2023).
- [71] C. Kim, G. D. Gu, and K. S. Burch, Evidence for Helical Hinge Zero Modes in an Fe-Based Superconductor, *Nano Lett.* **19**, 4890 (2019).
- [72] Y. Hwang, J. Ahn, and B.-J. Yang, Fragile topology protected by inversion symmetry: Diagnosis, bulk-boundary correspondence, and Wilson loop, *Phys. Rev. B* **100**, 205126 (2019).
- [73] J. Ahn, and B.-J. Yang, Higher-order topological superconductivity of spin-polarized fermions, *Phys. Rev. Research* **2**, 012060(R) (2020).
- [74] A. K. Ghosh, T. Nag, and A. Saha, Hierarchy of higher-order topological superconductors in three dimensions, *Phys. Rev. B* **104**, 134508 (2021).
- [75] B. Roy, and V. Jurićić, Mixed-parity octupolar pairing and corner Majorana modes in three dimensions, *Phys. Rev. B* **104**, L180503 (2021).
- [76] H. Watanabe, and H. C. Po, Fractional Corner Charge of Sodium Chloride, *Phys. Rev. X* **11**, 041064 (2021).
- [77] L. M. Vasiloiu, A. Tiwari, and J. H. Bardarson, Dephasing-enhanced Majorana zero modes in two-dimensional and three-dimensional higher-order topological superconductors, *Phys. Rev. B* **106**, L060307 (2022).
- [78] N. Mao, H. Wang, Y. Dai, B. Huang, and C. Niu, Third-order topological insulators with wallpaper fermions in  $\text{Ti}_4\text{PbTe}_3$  and  $\text{Ti}_4\text{SnTe}_3$ , *npj Computational Mater.* **8**, 154 (2022).
- [79] Z. Zhang, J. Ren, Y. Qi, and C. Fang, Topological classification of intrinsic three-dimensional superconductors using anomalous

- surface construction, *Phys. Rev. B* **106**, L121108 (2022).
- [80] X.-J. Luo and F. Wu, Generalization of Benalcazar-Bernevig-Hughes model to arbitrary dimensions, *Phys. Rev. B* **108**, 075143 (2023).
- [81] C.-K. Chiu, J. C. Y. Teo, A. P. Schnyder, and S. Ryu, Classification of topological quantum matter with symmetries, *Rev. Mod. Phys.* **88**, 035005 (2016).
- [82] C. Chan, L. Zhang, T. F. J. Poon, Y.-P. He, Y.-Q. Wang, and X.-J. Liu, Generic Theory for Majorana Zero Modes in 2D Superconductors, *Phys. Rev. Lett.* **119**, 047001 (2017).
- [83] See Supplemental Material for details on the derivation of Chern-Simons term  $\theta$ , the derivation of the two-particle Wess-Zumino term  $\tilde{n}_{WZ}$  and  $\tilde{n}_{WZ}$  mechanism for non-closed (pseudo)spin textures case, and the experimental schemes of realization of TOTIs and TOTSCs.
- [84] J. Wu, J. Liu, and X.-J. Liu, Topological Spin Texture in a Quantum Anomalous Hall Insulator, *Phys. Rev. Lett.* **113**, 136403 (2014).
- [85] R.-X. Zhang, H.-C. Hsu, and C.-X. Liu, Electrically tunable spin polarization of chiral edge modes in a quantum anomalous Hall insulator, *Phys. Rev. B* **93**, 235315 (2016).
- [86] Y. Tan, Z.-H. Huang, and X.-J. Liu, Two-particle Berry phase mechanism for Dirac and Majorana Kramers pairs of corner modes, *Phys. Rev. B* **105**, L041105 (2022).
- [87] Z. F. Wang, K.-H. Jin, and F. Liu, Quantum spin Hall phase in 2D trigonal lattice, *Nat. Commun.* **7**, 12746 (2016).
- [88] C. Wang, F. Liu, and H. Huang, Effective Model for Fractional Topological Corner Modes in Quasicrystals, *Phys. Rev. Lett.* **129**, 056403 (2022).
- [89] M. M. Sharma, P. Sharma, N. K. Karn and V. P. S. Awana, Comprehensive review on topological superconducting materials and interfaces, *Superconductor Science and Technology* **35**, 8 (2022).
- [90] Y. F. Li, X. Y. Xu, M.-H. Lee, M.-W. Chu, and C. L. Chien, Observation of half-quantum flux in the unconventional superconductor  $\beta$ -Bi<sub>2</sub>Pd, *Science* **366**, 6462 (2019).
- [91] A. Kolapo, T. Li, P. Hosur and J. H. M. Jr, Possible transport evidence for three-dimensional topological superconductivity in doped  $\beta$ -Bi<sub>2</sub>Pd, *Scientific Reports* **9**, 12504 (2019).
- [92] M. Sakano, K. Okawa, M. Kanou, H. Sanjo, T. Okuda, T. Sasagawa and K. Ishizaka, Topologically protected surface states in a centrosymmetric superconductor  $\beta$ -Bi<sub>2</sub>Pd, *Nat Commun* **6**, 8595 (2015).
- [93] I. R. Shein and A. L. Ivanovskii, Electronic band structure and Fermi surface of tetragonal low-temperature superconductor Bi<sub>2</sub>Pd as predicted from first principles, *Journal of Superconductivity and Novel Magnetism*, **26**, (2013).
- [94] R. S. K. Mong, A. M. Essin, and J. E. Moore, Antiferromagnetic topological insulators, *Phys. Rev. B* **81**, 245209 (2010).
- [95] D. Zhang, M. Shi, T. Zhu, D. Xing, H. Zhang, and J. Wang, Topological Axion States in the Magnetic Insulator MnBi<sub>2</sub>Te<sub>4</sub> with the Quantized Magnetoelectric Effect, *Phys. Rev. Lett.* **122**, 206401 (2019).
- [96] M. M. Otrokov, I. I. Klimovskikh, and H. Bentmann, Prediction and observation of an antiferromagnetic topological insulator, *Nature* **576**, 416 (2019).
- [97] S. Li, T. Liu, C. Liu, Y. Wang, H.-Z. Lu, and X. C. Xie, Progress on the antiferromagnetic topological insulator MnBi<sub>2</sub>Te<sub>4</sub>, *Nat Sci Rev* **11**, 2 (2023)
- [98] F. Tang, H. C. Po, A. Vishwanath, and X. Wan, Comprehensive search for topological materials using symmetry indicators, *Nature* **566**, 486 (2019).
- [99] Y. Xu, L. Elcoro, Z.-D. Song, B. J. Wieder, M. G. Vergniory, N. Regnault, Y. Chen, C. Felser, and B. A. Bernevig, High-throughput calculations of magnetic topological materials, *Nature* **586**, 702 (2020).

## Supplementary Material

In this supplementary material, we first compute the Chern-Simons (CS) term  $\tilde{\theta}$  analytically and demonstrate that a nonzero  $\tilde{\theta}$  can correspond to a zero corner mode (S-1). Next we derive the two-particle Wess-Zumino (WZ) term  $\tilde{n}_{\text{WZ}}$  based on (pseudo)spin textures defined on the surface of 3D topological insulators (TIs) or superconductors (TSCs) and introduce the  $\tilde{n}_{\text{WZ}}$  mechanism for closed and non-closed (pseudo)spin textures case in detail (S-2). In the end, we provide the feasible physical realization schemes for third-order topological insulators (TOTIs) and superconductors (TOTSCs), predicting the emergence of zero corner modes in terms of surface Chern-Simons theory ( $\tilde{\theta}$  characterization and  $\tilde{n}_{\text{WZ}}$  mechanism) (S-3). The symmetry analysis for zero corner modes are also provided.

### S-1. CHERN-SIMONS TERM $\tilde{\theta}$ CHARACTERIZATION FOR TOTIS (TOTSCS)

#### A. Chern-Simons term $\tilde{\theta}$

For 3D second-order topological insulators (SOTIs) or superconductors (SOTSCs), the effective surface Hamiltonian is usually given by:  $\mathcal{H}_{\text{effective}}^{\text{second}} = vk_1\Gamma_1 + vk_2\Gamma_2 + m_1\Gamma_3$  with  $\Gamma$  been gamma matrices, and the emergence of helical hinge modes relies on sign inversion of effective mass  $m_1$  of adjacent surfaces. In order to induce the 3rd-order zero energy corner modes from 3D SOTIs or SOTSCs, we also need to consider additional mass term  $m_2\Gamma_4$  which can gap out this helical hinge modes and change sign between adjacent hinges. Thus the effective surface Hamiltonian for 3D TOTIs or TOTSCs can be written as :  $\mathcal{H}_{\text{effective}}^{\text{3rd}} = vk_1\Gamma_1 + vk_2\Gamma_2 + m_1\Gamma_3 + m_2\Gamma_4$ , where  $\Gamma_i$  satisfies  $\{\Gamma_i, \Gamma_j\} = 2\delta_{ij}$ . Notice that  $\mathcal{H}_{\text{effective}} = vk_1\Gamma_1 + vk_2\Gamma_2$  represents the Dirac (Majorana) cones of 3D TIs (TSCs) and  $(m_1, m_2)$  can be viewed as surface effective mass field. In the following, we will show that the Chern-Simons term  $\tilde{\theta}$  is related two winding numbers derived from surface mass fields and Dirac (Majorana) cones of 3D TIs (TSCs).

As shown in Fig.S1(a), we focus on a sample corner  $c$  that is formed by three neighbouring surfaces (I), (II) and (III) of 3D TIs (TSCs). For simplicity, we adopt the spherical coordinate frame. Hence, the corresponding surface Dirac (Majorana) cone is captured by  $\mathcal{H}_{\text{effective}} = -k_\varphi\Gamma_1 + k_\theta\Gamma_2$ , where  $k_\varphi$  and  $k_\theta$  are momentums. Now we introduce the surface effective mass field  $(m_1, m_2)$  to  $\mathcal{H}_{\text{effective}}$  and compute the Chern-Simons term  $\tilde{\theta}$ . It is well known that  $\tilde{\theta}$  is defined on the manifold  $k^d \times \mathcal{M}^D$  with  $d + D = \text{odd}$  [1]. To meet this need, in addition to the 2D momentum space  $(k_\varphi, k_\theta)$ , we also focus on loop  $\mathcal{l}_\phi$  surrounding target corner  $c$  and take the real space parameter  $\phi$  as a synthetic dimension of ring geometry  $\mathcal{S}^1$ . When mass field  $(m_1, m_2)$  is parameterized as  $(B_\phi, M_\phi)$ , the  $\mathcal{H}_{\text{effective}}^{\text{3rd}}$  can be written down in a synthetic 3D space  $k^3 = k^2 \times \mathcal{S}^1$  spanned by  $(\mathbf{k}, \phi)$  with  $\mathcal{H}_{\text{effective}}^{\text{3rd}} = -k_\varphi\Gamma_1 + k_\theta\Gamma_2 + B_\phi\Gamma_3 + M_\phi\Gamma_4$ . Thus the Chern-Simons term with respect to corner  $c$  is given by

$$\tilde{\theta} = \frac{1}{4\pi} \int d^3k \epsilon_{abc} \text{tr} [\mathcal{A}_a \partial_b \mathcal{A}_c + i \frac{2}{3} \mathcal{A}_a \mathcal{A}_b \mathcal{A}_c], \quad (\text{S1})$$

where  $\mathcal{A}_{a=(\mathbf{k}, \phi), n, n'} = -i \langle \tilde{n} | \partial_a | \tilde{n}' \rangle$  is non-Abelian Berry connection with  $|\tilde{n}\rangle$  the eigenfunction for filled degenerate bands  $-E = -\sqrt{k_\varphi^2 + k_\theta^2 + B_\phi^2 + M_\phi^2}$ . In order to obtain the explicit form of  $|\tilde{n}\rangle$ ,  $\Gamma_i$  can be taken as  $\Gamma_1 = \mu_y \gamma_x$ ,  $\Gamma_2 = -\mu_y \gamma_z$ ,  $\Gamma_3 = \mu_y \gamma_y$ ,  $\Gamma_4 = \mu_x \gamma_0$ . As a result, the degenerate eigenvectors are given by  $|\tilde{1}\rangle = \begin{pmatrix} \frac{B_\phi - ik_\varphi}{\mathcal{N}} & \frac{-M_\phi + ik_\theta}{\mathcal{N}} & 0 & \frac{E}{\mathcal{N}} \end{pmatrix}^T$ ,  $|\tilde{2}\rangle = \begin{pmatrix} \frac{-M_\phi - ik_\theta}{\mathcal{N}} & \frac{-B_\phi - ik_\varphi}{\mathcal{N}} & \frac{E}{\mathcal{N}} & 0 \end{pmatrix}^T$  where  $\mathcal{N} = \sqrt{2E^2}$ . Correspondingly, the non-Abelian Berry connections are easily obtained:

$$\begin{aligned} \mathcal{A}_\phi &= -i \begin{pmatrix} \frac{(ik_\varphi)}{\mathcal{N}^2} & \frac{(M_\phi + ik_\theta)}{\mathcal{N}^2} \\ \frac{(-M_\phi + ik_\theta)}{\mathcal{N}^2} & \frac{(-ik_\varphi)}{\mathcal{N}^2} \end{pmatrix} \partial_\phi (B_\phi) - i \begin{pmatrix} \frac{(ik_\theta)}{\mathcal{N}^2} & \frac{-(B_\phi + ik_\varphi)}{\mathcal{N}^2} \\ \frac{(B_\phi - ik_\varphi)}{\mathcal{N}^2} & \frac{(-ik_\theta)}{\mathcal{N}^2} \end{pmatrix} \partial_\phi (M_\phi) \\ \mathcal{A}_{\mathbf{k}} &= -i \begin{pmatrix} \frac{-iB_\phi}{\mathcal{N}^2} & \frac{iM_\phi - k_\theta}{\mathcal{N}^2} \\ \frac{iM_\phi + k_\theta}{\mathcal{N}^2} & \frac{iB_\phi}{\mathcal{N}^2} \end{pmatrix} \nabla_{\mathbf{k}} (k_\varphi) - i \begin{pmatrix} \frac{-iM_\phi}{\mathcal{N}^2} & \frac{-iB_\phi + k_\varphi}{\mathcal{N}^2} \\ \frac{-iB_\phi - k_\varphi}{\mathcal{N}^2} & \frac{iM_\phi}{\mathcal{N}^2} \end{pmatrix} \nabla_{\mathbf{k}} (k_\theta). \end{aligned} \quad (\text{S2})$$

And the explicit form of  $\tilde{\theta}$  reads  $\frac{1}{4\pi} \int d^3k \text{tr} \{ [\mathcal{A}_{k_\varphi} (\partial_{k_\theta} \mathcal{A}_\phi - \partial_\phi \mathcal{A}_{k_\theta}) + \mathcal{A}_{k_\theta} (\partial_\phi \mathcal{A}_{k_\varphi} - \partial_{k_\varphi} \mathcal{A}_\phi) + \mathcal{A}_\phi (\partial_{k_\varphi} \mathcal{A}_{k_\theta} - \partial_{k_\theta} \mathcal{A}_{k_\varphi})] + i \frac{2}{3} [\mathcal{A}_{k_\varphi} (\mathcal{A}_{k_\theta} \mathcal{A}_\phi - \mathcal{A}_\phi \mathcal{A}_{k_\theta}) + \mathcal{A}_{k_\theta} (\mathcal{A}_\phi \mathcal{A}_{k_\varphi} - \mathcal{A}_{k_\varphi} \mathcal{A}_\phi) + \mathcal{A}_\phi (\mathcal{A}_{k_\varphi} \mathcal{A}_{k_\theta} - \mathcal{A}_{k_\theta} \mathcal{A}_{k_\varphi})] \}$ . To simplify the computation, we define four matrices  $\mathcal{A}_B, \mathcal{A}_M, \mathcal{A}_\varphi$  and  $\mathcal{A}_\theta$  which take the form of :

$$\begin{aligned} \mathcal{A}_B &= \begin{pmatrix} \frac{(ik_\varphi)}{\mathcal{N}^2} & \frac{(M_\phi + ik_\theta)}{\mathcal{N}^2} \\ \frac{(-M_\phi + ik_\theta)}{\mathcal{N}^2} & \frac{(-ik_\varphi)}{\mathcal{N}^2} \end{pmatrix}; & \mathcal{A}_M &= \begin{pmatrix} \frac{(ik_\theta)}{\mathcal{N}^2} & \frac{-(B_\phi + ik_\varphi)}{\mathcal{N}^2} \\ \frac{(B_\phi - ik_\varphi)}{\mathcal{N}^2} & \frac{(-ik_\theta)}{\mathcal{N}^2} \end{pmatrix} \\ \mathcal{A}_\varphi &= \begin{pmatrix} \frac{-iB_\phi}{\mathcal{N}^2} & \frac{iM_\phi - k_\theta}{\mathcal{N}^2} \\ \frac{iM_\phi + k_\theta}{\mathcal{N}^2} & \frac{iB_\phi}{\mathcal{N}^2} \end{pmatrix}; & \mathcal{A}_\theta &= \begin{pmatrix} \frac{-iM_\phi}{\mathcal{N}^2} & \frac{-iB_\phi + k_\varphi}{\mathcal{N}^2} \\ \frac{-iB_\phi - k_\varphi}{\mathcal{N}^2} & \frac{iM_\phi}{\mathcal{N}^2} \end{pmatrix}. \end{aligned} \quad (\text{S3})$$

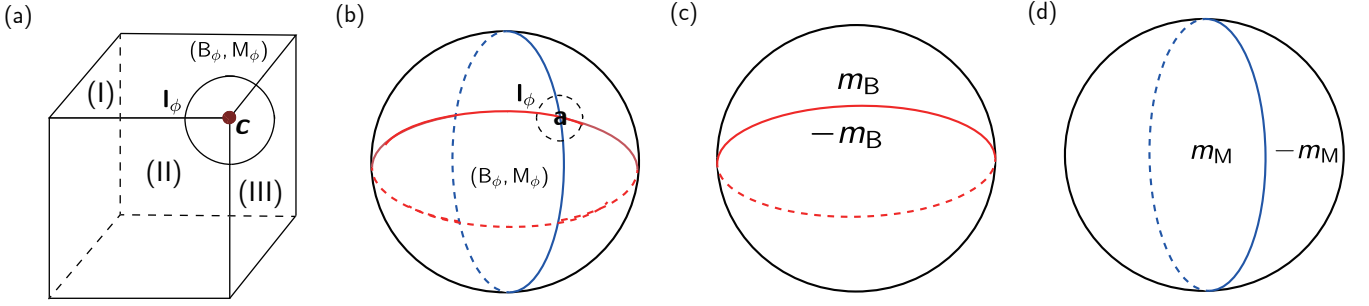


Figure S1. Chern-Simons term  $\tilde{\theta}$  characterization. (a) A schematic for effective mass field  $\mathbf{m} = (B_\phi, M_\phi)$  in the surface of 3D TI (TSC). Here (I), (II), (III) are three adjacent surfaces and corner  $\mathbf{c}$  is a common point of these surfaces.  $\mathbf{l}_\phi$  denotes a closed loop surrounding  $\mathbf{c}$ . (b) We can deform such surface effective mass field to that in (b) without gap closing. And the target corner  $\mathbf{c}$  is mapped to a intersection  $\mathbf{a}$  of the blue and red lines which represent respectively the mass domain walls formed by  $m_B$  in (c) and  $m_M$  in (d).

So the non-Abelian Berry connections are formulated as  $\mathcal{A}_{k_\varphi} = -i\mathcal{A}_\varphi$ ,  $\mathcal{A}_{k_\theta} = -i\mathcal{A}_\theta$  and  $\mathcal{A}_\phi = -i\mathcal{A}_{B_\phi} \partial_\phi(B_\phi) - i\mathcal{A}_{M_\phi} \partial_\phi(M_\phi)$ . Substituting them into the explicit form of  $\tilde{\theta}$ , we reach that  $\epsilon_{abc} \text{tr}[\mathcal{A}_a \partial_b \mathcal{A}_c + i\frac{2}{3} \mathcal{A}_a \mathcal{A}_b \mathcal{A}_c] = 2 \frac{M_\phi \partial_\phi(B_\phi) - B_\phi \partial_\phi(M_\phi)}{E^4}$ . Finally, the Chern-Simons term  $\tilde{\theta}$  can be expressed in a concise form:

$$\tilde{\theta} = \frac{1}{2\pi} \int_{-\infty}^{+\infty} \int_{-\infty}^{+\infty} \oint_{\mathbf{l}_\phi} d\mathbf{k}_\varphi d\mathbf{k}_\theta d\phi \frac{M_\phi \partial_\phi(B_\phi) - B_\phi \partial_\phi(M_\phi)}{(k_\varphi^2 + k_\theta^2 + B_\phi^2 + M_\phi^2)^2} = \pi \frac{1}{2\pi} \oint_{\mathbf{l}_\phi} d\phi \frac{M_\phi \partial_\phi(B_\phi) - B_\phi \partial_\phi(M_\phi)}{B_\phi^2 + M_\phi^2} = \pi \mathcal{W}_m, \quad (\text{S4})$$

where  $\mathbf{m} = (B_\phi, M_\phi)$  is the effective mass field defined on the surface of TOTIs (TOTSCs). Eq.(S4) shows that Chern-Simons term  $\tilde{\theta}$  is associated with the winding number of surface effective mass field  $\mathbf{m}$ . In fact,  $\tilde{\theta}$  is also dependent on the surface Dirac (Majorana) cone winding number in  $\mathbf{k}$  space besides the  $\mathcal{W}_m$ . To demonstrate this we consider a more general form:  $\mathcal{H}'_{\text{eff}} = h_1(k_\varphi, k_\theta) \mu_y \gamma_x + h_2(k_\varphi, k_\theta) \mu_y \gamma_z + B_\phi \mu_y \gamma_y + M_\phi \mu_x \gamma_0$  where  $\mathbf{h} = (h_1, h_2)$  is a linear function of  $\mathbf{k}$  (e.g.  $h_1 = -k_\varphi$ ,  $h_2 = -k_\theta$ ). Thus the corresponding degenerate ground states for  $\mathcal{H}'_{\text{eff}}$  become  $|\tilde{\text{I}}\rangle = \begin{pmatrix} \frac{B_\phi + ih_1}{\mathcal{N}} & \frac{-M_\phi + ih_2}{\mathcal{N}} & 0 & \frac{E}{\mathcal{N}} \end{pmatrix}^T$ ,  $|\tilde{\text{II}}\rangle = \begin{pmatrix} \frac{-M_\phi - ih_2}{\mathcal{N}} & \frac{-B_\phi + ih_1}{\mathcal{N}} & \frac{E}{\mathcal{N}} & 0 \end{pmatrix}^T$  with  $E = \sqrt{h_1^2 + h_2^2 + B_\phi^2 + M_\phi^2}$  and  $\mathcal{N} = \sqrt{2E^2}$ . Similarly, the non-Abelian Berry connections are given by  $\mathcal{A}_\phi = -i\mathcal{A}_{B_\phi} \partial_\phi(B_\phi) - i\mathcal{A}_{M_\phi} \partial_\phi(M_\phi)$ ,  $\mathcal{A}_{k_\varphi} = -i\mathcal{A}_1 \partial_{k_\varphi}(h_1) - i\mathcal{A}_2 \partial_{k_\varphi}(h_2)$ ,  $\mathcal{A}_{k_\theta} = -i\mathcal{A}_1 \partial_{k_\theta}(h_1) - i\mathcal{A}_2 \partial_{k_\theta}(h_2)$ . And  $\mathcal{A}_{B_\phi}$ ,  $\mathcal{A}_{M_\phi}$ ,  $\mathcal{A}_1$ ,  $\mathcal{A}_2$  read

$$\begin{aligned} \mathcal{A}_{B_\phi} &= \begin{pmatrix} \frac{(-ih_1)}{\mathcal{N}^2} & \frac{(M_\phi + ih_2)}{\mathcal{N}^2} \\ \frac{(-M_\phi + ih_2)}{\mathcal{N}^2} & \frac{(ih_1)}{\mathcal{N}^2} \end{pmatrix}; & \mathcal{A}_{M_\phi} &= \begin{pmatrix} \frac{(ih_2)}{\mathcal{N}^2} & \frac{(-B_\phi + ih_1)}{\mathcal{N}^2} \\ \frac{(B_\phi + ih_1)}{\mathcal{N}^2} & \frac{(-ih_2)}{\mathcal{N}^2} \end{pmatrix} \\ \mathcal{A}_1 &= \begin{pmatrix} \frac{(iB_\phi)}{\mathcal{N}^2} & \frac{(-iM_\phi + h_2)}{\mathcal{N}^2} \\ \frac{(-iM_\phi - h_2)}{\mathcal{N}^2} & \frac{-iB_\phi}{\mathcal{N}^2} \end{pmatrix}; & \mathcal{A}_2 &= \begin{pmatrix} \frac{(-iM_\phi)}{\mathcal{N}^2} & \frac{(-iB_\phi - h_1)}{\mathcal{N}^2} \\ \frac{(-iB_\phi + h_1)}{\mathcal{N}^2} & \frac{iM_\phi}{\mathcal{N}^2} \end{pmatrix}. \end{aligned} \quad (\text{S5})$$

After some algebraic operation, we obtain  $\epsilon_{abc} \text{tr}[\mathcal{A}_a \partial_b \mathcal{A}_c + i\frac{2}{3} \mathcal{A}_a \mathcal{A}_b \mathcal{A}_c] = \frac{2[\partial_{k_\varphi}(h_1) \partial_{k_\theta}(h_2) - \partial_{k_\theta}(h_1) \partial_{k_\varphi}(h_2)][M_\phi \partial_\phi(B_\phi) - B_\phi \partial_\phi(M_\phi)]}{E^4}$ . Then the Chern-Simons term  $\tilde{\theta}$  takes the form of

$$\begin{aligned} \tilde{\theta} &= \frac{1}{2\pi} \oint_{\mathbf{l}_\phi} d\phi \left[ \frac{M_\phi \partial_\phi(B_\phi) - B_\phi \partial_\phi(M_\phi)}{B_\phi^2 + M_\phi^2} \right] \int_{-\infty}^{+\infty} \int_{-\infty}^{+\infty} d\mathbf{k}_\varphi d\mathbf{k}_\theta \frac{[\partial_{k_\varphi}(h_1) \partial_{k_\theta}(h_2) - \partial_{k_\theta}(h_1) \partial_{k_\varphi}(h_2)](B_\phi^2 + M_\phi^2)}{E^4} \\ &= \mathcal{W}_m \int_{\mathbf{k} \text{ space}} \frac{d^2 \mathbf{k} \cdot (\nabla_{\mathbf{k}} h_1 \times \nabla_{\mathbf{k}} h_2) (B_\phi^2 + M_\phi^2)}{(h_1^2 + h_2^2 + B_\phi^2 + M_\phi^2)^2}. \end{aligned} \quad (\text{S6})$$

Both  $h_1$  and  $h_2$  depend linearly on  $\mathbf{k}$ , so  $\nabla_{\mathbf{k}} h_1(\mathbf{k}) \times \nabla_{\mathbf{k}} h_2(\mathbf{k})$  is a constant. And we have  $\int_{\mathbf{k} \text{ space}} \frac{d^2 \mathbf{k} \cdot (\nabla_{\mathbf{k}} h_1 \times \nabla_{\mathbf{k}} h_2) (B_\phi^2 + M_\phi^2)}{(h_1^2 + h_2^2 + B_\phi^2 + M_\phi^2)^2} = \int_{\mathbf{k} \text{ space} - \mathcal{S}} \frac{d^2 \mathbf{k} \cdot (\nabla_{\mathbf{k}} h_1 \times \nabla_{\mathbf{k}} h_2) (B_\phi^2 + M_\phi^2)}{(h_1^2 + h_2^2)^2}$  where  $\mathcal{S}$  denotes an area  $\{\mathbf{k} | h_1^2(\mathbf{k}) + h_2^2(\mathbf{k}) \leq B_\phi^2 + M_\phi^2\}$  in  $\mathbf{k}$  space and its boundary  $\partial \mathcal{S}$  is a closed loop along which  $h_1^2(\mathbf{k}) + h_2^2(\mathbf{k}) = B_\phi^2 + M_\phi^2$ . In other word,  $\partial \mathcal{S}$  resembles a ‘‘Fermi surface’’ which is obtained by crossing the Dirac (Majorana) cone with ‘‘chemical potential’’  $\mu = \sqrt{B_\phi^2 + M_\phi^2}$  (Fig.1(b) in main text). It is well known that  $\nabla_{\mathbf{k}} h_1 \times \nabla_{\mathbf{k}} h_2 = \nabla_{\mathbf{k}} \times (h_1 \nabla_{\mathbf{k}} h_2 - h_2 \nabla_{\mathbf{k}} h_1)$ , then Eq.(S6) becomes  $\tilde{\theta} = \mathcal{W}_m \int_{\mathbf{k} \text{ space} - \mathcal{S}} \frac{d^2 \mathbf{k} \cdot [\nabla_{\mathbf{k}} \times (h_1 \nabla_{\mathbf{k}} h_2 - h_2 \nabla_{\mathbf{k}} h_1)] (B_\phi^2 + M_\phi^2)}{(h_1^2 + h_2^2)^2}$ .

One can readily check that  $\nabla_{\mathbf{k}} \times \left[ \frac{h_2 \nabla_{\mathbf{k}} h_1 - h_1 \nabla_{\mathbf{k}} h_2}{2(h_1^2 + h_2^2)^2} \right] = \frac{[\nabla_{\mathbf{k}} \times (h_1 \nabla_{\mathbf{k}} h_2 - h_2 \nabla_{\mathbf{k}} h_1)]}{(h_1^2 + h_2^2)^2}$ . Hence

$$\tilde{\theta} = \mathcal{W}_m \int_{\mathbf{k} \text{ space-S}} d^2 \mathbf{k} \cdot \left\{ \nabla_{\mathbf{k}} \times \left[ \frac{h_2 \nabla_{\mathbf{k}} h_1 - h_1 \nabla_{\mathbf{k}} h_2}{2(h_1^2 + h_2^2)^2} \right] \right\} (B_\phi^2 + M_\phi^2). \quad (\text{S7})$$

Using the Stokes' theorem, we obtain

$$\tilde{\theta} = \pi \mathcal{W}_m \frac{1}{2\pi} \oint_{\partial S} \frac{d\mathbf{l} \cdot (h_2 \nabla_{\mathbf{k}} h_1 - h_1 \nabla_{\mathbf{k}} h_2)}{(h_2^2 + h_1^2)} = \pi \mathcal{W}_h \mathcal{W}_m, \quad (\text{S8})$$

where  $\mathcal{W}_h$  denotes the Dirac (Majorana) cone winding number in  $\mathbf{k}$  space. So far, we have shown that the CS term  $\tilde{\theta}$ , which is defined within a synthetic 3D space  $(\mathbf{k}, \phi)$ , relies on two winding numbers derived from surface mass fields and Dirac (Majorana) cones. Furthermore, Eq.(S8) also shows that Chern-Simons term can reduce to the Hopf invariant which captures the linking number of the inverse images of two points in the target space  $S^2$  of effective surface Hamiltonian  $\mathcal{H}_{\text{effective}}(\mathbf{k}, \phi)$  [2]. In general, for Dirac (Majorana) cone dictated by the Hamiltonian  $\mathbf{h} \cdot \Gamma$  (e.g.  $h_1 = -k_\varphi$ ,  $h_2 = k_\theta$ ),  $\mathcal{W}_h = 1$ , so  $\tilde{\theta}$  returns to Eq.(S4).

### B. The relation between nonzero $\tilde{\theta}$ and zero corner mode

In the previous discussion, we have got the Chern-Simons term which reads  $\tilde{\theta} = \pi \mathcal{W}_h \mathcal{W}_m$ . Now we will demonstrate that a nonzero  $\tilde{\theta}$  can correspond to a zero corner mode. For convenience, we deform the cubic sample in Fig.S1(a) to a sphere shown in Fig.S1(b) without gap closing, thus target corner  $c$  is correspondingly mapped to the intersection  $a$ . Now we first focus on sphere sample and consider the following effective Hamiltonian:

$$\mathcal{H}_{\text{eff}} = -k_\varphi \mu_y \gamma_x - k_\theta \mu_y \gamma_z + m_B(\theta) \mu_x \gamma_0 - m_M(\varphi) \mu_y \gamma_y. \quad (\text{S9})$$

According to the discussion in [3, 4], we can obtain the zero-energy localized solution. As plotted in Fig.S1(c), we will treat the  $\theta$ -edge as a domain wall where  $m_B$  steps from positive (inside the topological phase) to negative (outside the topological phase):  $m_B(\theta) > 0$  (topological,  $\theta < \theta_0$ ),  $m_B(\theta) < 0$  (trivial,  $\theta_0 > \theta$ ) and find the equation  $(i\partial_\theta \mu_y \gamma_z + m_B(\theta) \mu_x \gamma_0) \Psi(\theta) = 0$ . With the ansatz  $\Psi(\theta) = \exp(\int_{\theta_0}^\theta m_B(\theta') d\theta') \Phi_\theta$  for some constant spinor  $\Phi_\theta$ , the matrix equation can be simplified to  $(I - \mu_z \otimes \gamma_z) \Phi_x = 0$  and two solutions  $\Phi_{\theta 1} = (1, 0, 0, 0)^T$ ,  $\Phi_{\theta 2} = (0, 0, 0, 1)^T$  which correspond to the positive eigenstate of  $\mu_z \otimes \gamma_z$  are obtained. Then we project the rest of the Hamiltonian ( $\mathcal{H}_{\text{rest}} = -k_\varphi \mu_y \gamma_x - m_M(\varphi) \mu_y \gamma_y$ ) in Eq.(S9) onto the subspace spanned by  $|\Phi_{\theta 1}\rangle$  and  $|\Phi_{\theta 2}\rangle$  to find the edge Hamiltonian  $\mathcal{H}_{\text{edge}, \theta}$

$$\mathcal{H}_{\text{edge}, \theta} = \begin{pmatrix} \langle \Phi_{\theta 1} | \mathcal{H}_{\text{rest}} | \Phi_{\theta 1} \rangle & \langle \Phi_{\theta 1} | \mathcal{H}_{\text{rest}} | \Phi_{\theta 2} \rangle \\ \langle \Phi_{\theta 2} | \mathcal{H}_{\text{rest}} | \Phi_{\theta 1} \rangle & \langle \Phi_{\theta 2} | \mathcal{H}_{\text{rest}} | \Phi_{\theta 2} \rangle \end{pmatrix} = -k_\varphi \tau_y + m_M(\varphi) \tau_x. \quad (\text{S10})$$

Similarly, we also reach  $\mathcal{H}_{\text{edge}, \varphi} = -k_\theta \nu_y + m_B(\theta) \nu_x$  [Fig.S1(d)]. Now, we can get the simultaneous zero mode by considering a intersection, i.e., either an  $\theta$ -edge with a  $\varphi$  domain wall or a  $\varphi$ -edge with an  $\theta$  domain wall. Further, we find the following two matrix equations for such two configurations respectively:  $(I - \tilde{\tau}_z) \phi_{\varphi, \theta} = 0$  and  $(I - \tilde{\nu}_z) \phi_{\theta, \varphi} = 0$ . As a result, the zero mode  $\Phi = \begin{pmatrix} 1 \\ 0 \end{pmatrix}$  for an  $\theta$ -edge with a  $\varphi$  domain wall is the positive eigenstate of  $\tilde{\tau}_z$  while that for the  $\varphi$ -edge with a  $\theta$  domain wall is the positive eigenstate of  $\tilde{\nu}_z$ . That is to say, the zero mode is a simultaneous zero mode of  $\mathcal{H}_{\text{edge}, \theta}$  and  $\mathcal{H}_{\text{edge}, \varphi}$ , which indicates a single mode appears at the intersection.

We have illustrated that a zero mode emerges at the intersection of two domain walls under the mass configurations considered above:  $m_B(\theta) > 0$  (topological,  $\theta < \theta_0$ );  $m_B(\theta) < 0$  (trivial,  $\theta_0 > \theta$ ) and  $m_M(\varphi) > 0$  (topological,  $\varphi < \varphi_0$ );  $m_M(\varphi) < 0$  (trivial,  $\varphi_0 > \varphi$ ). Next, we compute the Chern-Simons term  $\tilde{\theta}$ . Since  $\mathcal{H}_{\text{eff}}^h = -k_\varphi \mu_y \gamma_x - k_\theta \mu_y \gamma_z$  is a Dirac-type Hamiltonian, we can readily show that  $\mathcal{W}_h = 1$ . Additionally, to obtain the winding number  $\mathcal{W}_m$  of such effective mass field  $\mathbf{m}$ ,  $\phi \in [0, 2\pi)$  [Fig.S1(b)] is adopted to parameterize the  $\mathbf{m}$ . Specifically,  $m_B(\theta) \Rightarrow m_B \cos \phi$  and  $m_M(\varphi) \Rightarrow m_M \sin \phi$ , where  $m_B = m_M = m$ . According to Eq.(S4), the Chern-Simons term is computed:

$$\tilde{\theta} = \pi \mathcal{W}_h \mathcal{W}_m = \pi \left[ \frac{1}{2\pi} \int_0^{2\pi} d\phi \frac{-m^2 \sin \phi \partial_\phi (\cos \phi) + m^2 \cos \phi \partial_\phi (\sin \phi)}{m^2} \right] = \frac{1}{2} \int_0^{2\pi} d\phi = \pi \quad (\text{S11})$$

In contrast, we also calculate the  $\tilde{\theta}$  for a different effective mass field  $\mathbf{m}'$  which can't enable the emergence of a zero mode:  $m_B(\theta) \Rightarrow -m_B \cos \phi$  and  $m_M(\varphi) \Rightarrow -m_M \cos \phi$ . Hence we obtain

$$\tilde{\theta}' = \pi \mathcal{W}_h' \mathcal{W}_m' = \pi \left[ \frac{1}{2\pi} \int_0^{2\pi} d\phi \frac{m^2 \cos \phi \partial_\phi (\cos \phi) - m^2 \cos \phi \partial_\phi (\cos \phi)}{m^2} \right] = 0 \quad (\text{S12})$$

Till now, we have shown that the existence of zero mode at intersection of domain walls is related to the Chern-Simons term  $\tilde{\theta}$ . Owing to the fact that the cube and sphere are topologically equivalent and the corner  $c$  is mapped to the intersection  $a$  after such deformation, a zero mode at  $a$  must correspond to a zero mode at corner  $c$ , leading to the TOTIs (TOTSCs). In other word, a topologically protected zero corner mode is characterized by a nonzero Chern-Simons term ( $\tilde{\theta} = \pi$ ). And since the effective surface Hamiltonian of TOTIs (TOTSCs) resembles that of the 2D  $p \pm ip$  superconductors with Majorana zero mode at the vortex core, it belongs to the class D of tenfold classification. Finally, it is noteworthy that the characterization theory based on  $\tilde{\theta}$  is built on the general surface effective Hamiltonian, rather than the specific detailed bulk properties. Consequently, this approach is applicable to all TOTIs and TOTSCs, irrespective of the methods used to achieve these topological phases. In conclusion, it stands as a robust characterization theory that unifies the understanding of zero corner modes in both TOTIs and TOTSCs.

## S-2. TWO-PARTICLE WESS-ZUMINO TERM $\tilde{n}_{\text{WZ}}$ MECHANISM FOR TOTIS (TOTSCS)

### A. Two-particle Wess-Zumino term $\tilde{n}_{\text{WZ}}$

In this section, We derive the two-particle Wess-Zumino term  $\tilde{n}_{\text{WZ}}$  which is defined on the surface of 3D TIs (TSCs). As discussed in [5], the trajectories of pseudospins  $\mathbf{n}_\uparrow$  and  $\mathbf{n}_\downarrow$  of 2D quantum spin Hall insulators from one edge to adjacent one jointly form a closed loop (circle) under the ideal condition, which enables the appearance of two-particle Berry phase. Naturally, when we focus on 3D TIs (TSCs), the surface (pseudo)spin textures around target corner are expected to constitute a perfect sphere and may also contribute to an interesting topological invariant. To demonstrate this we concentrate on an area  $S$  of surface of 3D TIs (TSCs) with its center locating in corner  $a$  [Fig.S2(a)] and study the topological structure of surface (pseudo)spin textures defined on it. For a minimal 3D  $\mathcal{T}$ -invariant 3D TIs (TSCs), the spinor parts of topological surface states usually take the form of

$$|\tilde{\epsilon}_1\rangle = \frac{1}{\sqrt{2}} \begin{pmatrix} 1 \\ -i \end{pmatrix}_{\sigma(\tau)} \otimes \begin{pmatrix} \cos \theta/2 \\ e^{i\varphi} \sin \theta/2 \end{pmatrix}_s; \quad |\tilde{\epsilon}_2\rangle = \frac{1}{\sqrt{2}} \begin{pmatrix} 1 \\ i \end{pmatrix}_{\sigma(\tau)} \otimes \begin{pmatrix} \sin \theta/2 \\ -e^{i\varphi} \cos \theta/2 \end{pmatrix}_s, \quad (\text{S13})$$

where  $\theta(\varphi)$  represents the polar (azimuthal) angle in real space. Notice that  $\sigma, \tau$  and  $s$  denote the pseudospin, Nambu and spin degrees of freedom, respectively. Now we can define the surface (pseudo)spin polarizations:  $\mathbf{n}_1 = \langle \tilde{\epsilon}_1 | \mathbf{s} | \tilde{\epsilon}_1 \rangle$ ,  $\mathbf{n}_2 = \langle \tilde{\epsilon}_2 | \mathbf{s} | \tilde{\epsilon}_2 \rangle$ . Here  $\mathbf{n}_1 = -\mathbf{n}_2$  since  $\langle \tilde{\epsilon}_1 | \mathbf{s} | \tilde{\epsilon}_1 \rangle = \langle \tilde{\epsilon}_2 | \hat{\mathcal{T}}^{-1} \mathbf{s} \hat{\mathcal{T}} | \tilde{\epsilon}_2 \rangle = -\langle \tilde{\epsilon}_2 | \mathbf{s} | \tilde{\epsilon}_2 \rangle$ . And we find that (pseudo)spin  $\mathbf{n}_1 = (\sin \theta \cos \varphi, \sin \theta \sin \varphi, \cos \theta)$  is coincident with the surface normal vector  $e_r$  of 3D TIs (TSCs). As shown in [Fig.S2(b)], only one  $\mathbf{n}_{\nu=(1,2)}$  within  $S$  doesn't form a perfect sphere, but the joint textures of two polarizations  $\mathbf{n}_1$  and  $\mathbf{n}_2$  can constitute a "two-particle" unit sphere  $\tilde{S}_1 + \tilde{S}_2$  in (pseudo)spin space under ideal condition, resembling a hedgehog ball. Thus we can define a two-particle WZ term on  $S$ :

$$\tilde{n}_{\text{WZ}} = \frac{1}{2\pi} \int_S d\theta d\varphi (\partial_\theta \tilde{\mathcal{A}}_\varphi - \partial_\varphi \tilde{\mathcal{A}}_\theta), \quad (\text{S14})$$

where  $\tilde{\mathcal{A}}_\theta = \langle \tilde{\epsilon}_1 | \otimes \langle \tilde{\epsilon}_2 | (-i\partial_\theta) | \tilde{\epsilon}_1 \rangle \otimes | \tilde{\epsilon}_2 \rangle$ ,  $\tilde{\mathcal{A}}_\varphi = \langle \tilde{\epsilon}_1 | \otimes \langle \tilde{\epsilon}_2 | (-i\partial_\varphi) | \tilde{\epsilon}_1 \rangle \otimes | \tilde{\epsilon}_2 \rangle$  denote the two-particle Berry connections. Performing a transformation from real space to (pseudo)spin space:

$$\begin{aligned} \langle \tilde{\epsilon}_1 | \otimes \langle \tilde{\epsilon}_2 | (-i\partial_\theta) | \tilde{\epsilon}_1 \rangle \otimes | \tilde{\epsilon}_2 \rangle &= \frac{\partial \bar{\theta}_1}{\partial \theta} \langle \tilde{\epsilon}_1 | (-i\partial_{\bar{\theta}_1}) | \tilde{\epsilon}_1 \rangle + \frac{\partial \bar{\theta}_2}{\partial \theta} \langle \tilde{\epsilon}_2 | (-i\partial_{\bar{\theta}_2}) | \tilde{\epsilon}_2 \rangle \\ \langle \tilde{\epsilon}_1 | \otimes \langle \tilde{\epsilon}_2 | (-i\partial_\varphi) | \tilde{\epsilon}_1 \rangle \otimes | \tilde{\epsilon}_2 \rangle &= \frac{\partial \bar{\varphi}_1}{\partial \varphi} \langle \tilde{\epsilon}_1 | (-i\partial_{\bar{\varphi}_1}) | \tilde{\epsilon}_1 \rangle + \frac{\partial \bar{\varphi}_2}{\partial \varphi} \langle \tilde{\epsilon}_2 | (-i\partial_{\bar{\varphi}_2}) | \tilde{\epsilon}_2 \rangle, \end{aligned} \quad (\text{S15})$$

we obtain  $\tilde{\mathcal{A}}_\theta = \frac{\partial \bar{\theta}_1}{\partial \theta} \tilde{\mathcal{A}}_{\bar{\theta}_1} + \frac{\partial \bar{\theta}_2}{\partial \theta} \tilde{\mathcal{A}}_{\bar{\theta}_2}$ ,  $\tilde{\mathcal{A}}_\varphi = \frac{\partial \bar{\varphi}_1}{\partial \varphi} \tilde{\mathcal{A}}_{\bar{\varphi}_1} + \frac{\partial \bar{\varphi}_2}{\partial \varphi} \tilde{\mathcal{A}}_{\bar{\varphi}_2}$  with  $\tilde{\mathcal{A}}_{\bar{\theta}_i(\bar{\varphi}_i)} = \langle \tilde{\epsilon}_i | (-i\partial_{\bar{\theta}_i(\bar{\varphi}_i)}) | \tilde{\epsilon}_i \rangle$ . Here we emphasize that  $\bar{\theta}_i$  and  $\bar{\varphi}_i$  are the polar and azimuthal angles with respect to  $e_{\bar{z}}$  in (pseudo)spin space. Notice that  $e_{\bar{z}}$  is chosen as the vector  $e_{r=r_a}$  from "center of  $\partial S$ " to corner  $a$ , where "center of  $\partial S$ " is defined as the center of section obtained by cutting corner  $a$  along

$\partial\mathcal{S}$ . Substituting Eq.(S15) into (S14), we find that

$$\begin{aligned}
\tilde{n}_{\text{WZ}} &= \frac{1}{2\pi} \int_{\mathcal{S}} d\theta d\varphi [\partial_{\theta} \tilde{\mathcal{A}}_{\varphi} - \partial_{\varphi} \tilde{\mathcal{A}}_{\theta}] \\
&= \frac{1}{2\pi} \int_{\mathcal{S}} d\theta d\varphi [\partial_{\theta} (\frac{\partial \bar{\varphi}_1}{\partial \varphi} \tilde{\mathcal{A}}_{\bar{\varphi}_1} + \frac{\partial \bar{\varphi}_2}{\partial \varphi} \tilde{\mathcal{A}}_{\bar{\varphi}_2}) - \partial_{\varphi} (\frac{\partial \bar{\theta}_1}{\partial \theta} \tilde{\mathcal{A}}_{\bar{\theta}_1} + \frac{\partial \bar{\theta}_2}{\partial \theta} \tilde{\mathcal{A}}_{\bar{\theta}_2})] \\
&= \frac{1}{2\pi} \int_{\mathcal{S}} d\theta d\varphi [(\partial_{\theta} \frac{\partial \bar{\varphi}_1}{\partial \varphi} \tilde{\mathcal{A}}_{\bar{\varphi}_1} - \partial_{\varphi} \frac{\partial \bar{\theta}_1}{\partial \theta} \tilde{\mathcal{A}}_{\bar{\theta}_1}) + (\partial_{\theta} \frac{\partial \bar{\varphi}_2}{\partial \varphi} \tilde{\mathcal{A}}_{\bar{\varphi}_2} - \partial_{\varphi} \frac{\partial \bar{\theta}_2}{\partial \theta} \tilde{\mathcal{A}}_{\bar{\theta}_2})] \\
&= \frac{1}{2\pi} \int_{\mathcal{S}} d\theta d\varphi [(\frac{\partial \bar{\theta}_1}{\partial \theta} \frac{\partial \bar{\varphi}_1}{\partial \varphi} \partial_{\bar{\theta}_1} \tilde{\mathcal{A}}_{\bar{\varphi}_1} - \frac{\partial \bar{\theta}_1}{\partial \theta} \frac{\partial \bar{\varphi}_1}{\partial \varphi} \partial_{\bar{\varphi}_1} \tilde{\mathcal{A}}_{\bar{\theta}_1}) + (\frac{\partial \bar{\theta}_2}{\partial \theta} \frac{\partial \bar{\varphi}_2}{\partial \varphi} \partial_{\bar{\theta}_2} \tilde{\mathcal{A}}_{\bar{\varphi}_2} - \frac{\partial \bar{\theta}_2}{\partial \theta} \frac{\partial \bar{\varphi}_2}{\partial \varphi} \partial_{\bar{\varphi}_2} \tilde{\mathcal{A}}_{\bar{\theta}_2})] \\
&= \frac{1}{2\pi} \int_{\mathcal{S}} d\theta d\varphi \frac{\partial \bar{\theta}_1}{\partial \theta} \frac{\partial \bar{\varphi}_1}{\partial \varphi} (\partial_{\bar{\theta}_1} \tilde{\mathcal{A}}_{\bar{\varphi}_1} - \partial_{\bar{\varphi}_1} \tilde{\mathcal{A}}_{\bar{\theta}_1}) + \frac{1}{2\pi} \int_{\mathcal{S}} d\theta d\varphi \frac{\partial \bar{\theta}_2}{\partial \theta} \frac{\partial \bar{\varphi}_2}{\partial \varphi} (\partial_{\bar{\theta}_2} \tilde{\mathcal{A}}_{\bar{\varphi}_2} - \partial_{\bar{\varphi}_2} \tilde{\mathcal{A}}_{\bar{\theta}_2}) \\
&= \frac{1}{2\pi} \int_{\bar{\mathcal{S}}_1} d\bar{\theta}_1 d\bar{\varphi}_1 (\partial_{\bar{\theta}_1} \tilde{\mathcal{A}}_{\bar{\varphi}_1} - \partial_{\bar{\varphi}_1} \tilde{\mathcal{A}}_{\bar{\theta}_1}) + \frac{1}{2\pi} \int_{\bar{\mathcal{S}}_2} d\bar{\theta}_2 d\bar{\varphi}_2 (\partial_{\bar{\theta}_2} \tilde{\mathcal{A}}_{\bar{\varphi}_2} - \partial_{\bar{\varphi}_2} \tilde{\mathcal{A}}_{\bar{\theta}_2}) \\
&= \frac{1}{2\pi} \int_{\bar{\mathcal{S}}_1} d\bar{\theta}_1 d\bar{\varphi}_1 \tilde{\mathcal{B}}_{\bar{\theta}_1 \bar{\varphi}_1} + \frac{1}{2\pi} \int_{\bar{\mathcal{S}}_2} d\bar{\theta}_2 d\bar{\varphi}_2 \tilde{\mathcal{B}}_{\bar{\theta}_2 \bar{\varphi}_2} \\
&= \frac{1}{2\pi} \int_{\bar{\mathcal{S}}_1} d\bar{\theta}_1 d\bar{\varphi}_1 [-i(\langle \partial_{\bar{\theta}_1} \tilde{\varepsilon}_1 | \partial_{\bar{\varphi}_1} \tilde{\varepsilon}_1 \rangle - \langle \partial_{\bar{\varphi}_1} \tilde{\varepsilon}_1 | \partial_{\bar{\theta}_1} \tilde{\varepsilon}_1 \rangle)] + \frac{1}{2\pi} \int_{\bar{\mathcal{S}}_2} d\bar{\theta}_2 d\bar{\varphi}_2 [-i(\langle \partial_{\bar{\theta}_2} \tilde{\varepsilon}_2 | \partial_{\bar{\varphi}_2} \tilde{\varepsilon}_2 \rangle - \langle \partial_{\bar{\varphi}_2} \tilde{\varepsilon}_2 | \partial_{\bar{\theta}_2} \tilde{\varepsilon}_2 \rangle)], \quad (\text{S16})
\end{aligned}$$

where  $\bar{\theta}_2 = \pi - \bar{\theta}_1$ ,  $\bar{\varphi}_2 = \pi + \bar{\varphi}_1$ . Using the relation  $-i(\langle \partial_{\theta_{\mu}} \varepsilon_{\mu} | \partial_{\varphi_{\mu}} \varepsilon_{\mu} \rangle - \langle \partial_{\varphi_{\mu}} \varepsilon_{\mu} | \partial_{\theta_{\mu}} \varepsilon_{\mu} \rangle) = (-i) \text{tr} \epsilon_{\theta_{\mu} \varphi_{\mu}} (P_{\mu} \partial_{\theta_{\mu}} P_{\mu} \partial_{\varphi_{\mu}} P_{\mu}) = \frac{\mu}{2} \mathbf{e}_{\mathbf{r}} \cdot (\partial_{\theta_{\mu}} \mathbf{e}_{\mathbf{r}} \times \partial_{\varphi_{\mu}} \mathbf{e}_{\mathbf{r}})$  with  $\mu = 1, 2$  and  $P_{\mu} = \frac{1}{2}(1 + \mu \sum_i e_i s_i)$ , the two-particle Wess-Zumino term  $\tilde{n}_{\text{WZ}}$  becomes

$$\tilde{n}_{\text{WZ}} = \frac{1}{4\pi} \left\{ \int_{\bar{\mathcal{S}}_1} d\bar{\theta}_1 d\bar{\varphi}_1 [\mathbf{n}_1 \cdot (\partial_{\bar{\theta}_1} \mathbf{n}_1 \times \partial_{\bar{\varphi}_1} \mathbf{n}_1)] + \int_{\bar{\mathcal{S}}_2} d\bar{\theta}_2 d\bar{\varphi}_2 [\mathbf{n}_2 \cdot (\partial_{\bar{\theta}_2} \mathbf{n}_2 \times \partial_{\bar{\varphi}_2} \mathbf{n}_2)] \right\}. \quad (\text{S17})$$

Here  $\bar{\mathcal{S}}_1 + \bar{\mathcal{S}}_2$  represents a unit spherical surface in (pseudo)spin space with  $|\bar{\mathcal{S}}_1| = |\bar{\mathcal{S}}_2|$ . Since  $\int_{\bar{\mathcal{S}}_1} d\bar{\Omega}_1 + \int_{\bar{\mathcal{S}}_2} d\bar{\Omega}_2 = \int_{\bar{\mathcal{S}}_1} d\bar{\Omega}_1 + \int_{-\bar{\mathcal{S}}_2} (-d\bar{\Omega}_1)$ , we have

$$\begin{aligned}
\tilde{n}_{\text{WZ}} &= \frac{1}{4\pi} \int_{\bar{\mathcal{S}}_1} d\bar{\theta}_1 d\bar{\varphi}_1 [\mathbf{n}_1 \cdot (\partial_{\bar{\theta}_1} \mathbf{n}_1 \times \partial_{\bar{\varphi}_1} \mathbf{n}_1)] + \frac{1}{4\pi} \int_{-\bar{\mathcal{S}}_2} d\bar{\theta}_1 \frac{\partial \bar{\theta}_2}{\partial \bar{\theta}_1} d\bar{\varphi}_1 \frac{\partial \bar{\varphi}_2}{\partial \bar{\varphi}_1} [\mathbf{n}_2 \cdot (\frac{\partial \bar{\theta}_2}{\partial \bar{\theta}_1} \partial_{\bar{\theta}_1} \mathbf{n}_2 \times \frac{\partial \bar{\varphi}_2}{\partial \bar{\varphi}_1} \partial_{\bar{\varphi}_1} \mathbf{n}_2)] \\
&= \frac{1}{4\pi} \int_{\bar{\mathcal{S}}_1} d\bar{\theta}_1 d\bar{\varphi}_1 [\mathbf{n}_1 \cdot (\partial_{\bar{\theta}_1} \mathbf{n}_1 \times \partial_{\bar{\varphi}_1} \mathbf{n}_1)] - \frac{1}{4\pi} \int_{-\bar{\mathcal{S}}_2} d\bar{\theta}_1 d\bar{\varphi}_1 [\mathbf{n}_1 \cdot (\partial_{\bar{\theta}_1} \mathbf{n}_1 \times \partial_{\bar{\varphi}_1} \mathbf{n}_1)] \\
&= \frac{1}{4\pi} \int_{\bar{\mathcal{S}}_1 - (-\bar{\mathcal{S}}_2)} d\bar{\theta}_1 d\bar{\varphi}_1 [\mathbf{n}_1 \cdot (\partial_{\bar{\theta}_1} \mathbf{n}_1 \times \partial_{\bar{\varphi}_1} \mathbf{n}_1)] \\
&= \frac{1}{4\pi} \int_{\text{sphere}} d\bar{\theta} d\bar{\varphi} [\mathbf{e}_{\bar{\mathbf{r}}} \cdot (\partial_{\bar{\theta}} \mathbf{e}_{\bar{\mathbf{r}}} \times \partial_{\bar{\varphi}} \mathbf{e}_{\bar{\mathbf{r}}})]. \quad (\text{S18})
\end{aligned}$$

As we can see, Eq.(S18) returns to the general form of Wess-Zumino term  $n_{\text{WZ}}$ , which explains that why Eq.(S17) can be dubbed the two-particle Wess-Zumino term  $\tilde{n}_{\text{WZ}}$ .

## B. Two-particle Wess-Zumino term $\tilde{n}_{\text{WZ}}$ mechanism

Before proceeding, we emphasize that 3D TIs (TSCs) described by a minimal  $4 \times 4$  tight-binding Hamiltonian  $\mathcal{H}(\mathbf{k})$  can't harbour the 3rd-order zero corner modes as only one effective surface mass term  $m\sigma_k$  can gap out the surface Dirac (Majorana) cone captured by  $\mathcal{H} = k_x \sigma_x + k_y \sigma_y$ , where  $\sigma_i$  is the Pauli Matrix. In order to construct the TOTIs and TOTSCs, we need to stack two copies of minimal 3D TIs (TSCs), which is dubbed the ‘‘double-TI (TSC)’’ construction [6–8]. And the surface Dirac (Majorana) cone is given by  $\mathcal{H}' = k_x \Gamma_1 + k_y \Gamma_2$  with  $\Gamma$  been gamma matrices. Then we can apply a mass field  $m_B \Gamma_3 + m_M \Gamma_4$  to gap out such surface Dirac (Majorana) cone, leading to the zero energy corner modes.

Now we show the  $\tilde{n}_{\text{WZ}}$  mechanism for 3rd-order zero corner modes of TOTIs (TOTSCs). First, we construct the 3D total TIs (TSCs) by stacking two identical time-reversal invariant TIs (TSCs)  $\mathcal{H}_{\text{TI(TSC)}}^{\text{total}} = \mathcal{H}_{\text{TI(TSC)}}^{\alpha} \oplus \mathcal{H}_{\text{TI(TSC)}}^{\beta}$ , where  $\mathcal{H}_{\text{TI(TSC)}}^{\alpha(\beta)}$  is the minimal  $4 \times 4$  tight-binding Hamiltonian. Hence the surface (pseudo)spin polarizations are grouped into  $\{\mathbf{n}_1, \mathbf{n}_2\}_{\alpha}$  and

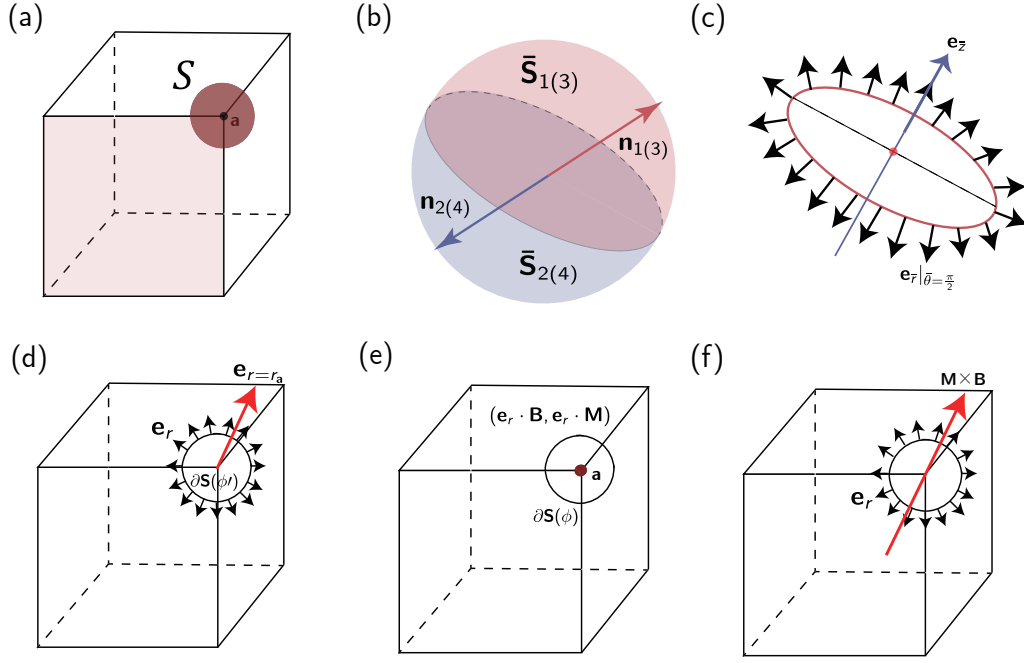


Figure S2. Two-particle Wess-Zumino term  $\tilde{n}_{\text{WZ}}$  mechanism. (a) Area  $S$  centered at corner  $a$ . (b) Surface (pseudo)spin textures within  $S$ . The red and blue hemispherical surfaces ( $\bar{S}_{1(3)}$  and  $\bar{S}_{2(4)}$ ) denote the textures of (pseudo)spin polarizations  $\mathbf{n}_{1(3)}$  (red arrow) and  $\mathbf{n}_{2(4)}$  (blue arrow) under the ideal condition, respectively. Here  $\bar{S}_{1(3)} + \bar{S}_{2(4)}$  make up a perfect unit sphere which renders the  $\tilde{n}_{\text{WZ}}$ . (c) The  $\tilde{n}_{\text{WZ}}$  can reduce to a winding number of  $e_{\bar{r}}|_{\bar{\theta}=\frac{\pi}{2}}$  on the equator of  $\bar{S}_{1(3)} + \bar{S}_{2(4)}$ . Vector  $e_{r=r_a}$  in real space is taken as  $e_{\bar{z}}$  in (pseudo)spin space. (d) The winding of  $e_{\bar{r}}|_{\bar{\theta}=\frac{\pi}{2}}$  can be mapped to that of  $e_r$  along the boundary  $\partial S$  in real space. (e) A specialized mass field  $(B_\phi, M_\phi) = (e_r \cdot \mathbf{B}, e_r \cdot \mathbf{M})$  is placed on the surface of 3D TI (TSC). (f) A nonzero CS term  $\tilde{\theta}$  can be caused by the winding of  $e_r$  along  $\partial S$ .

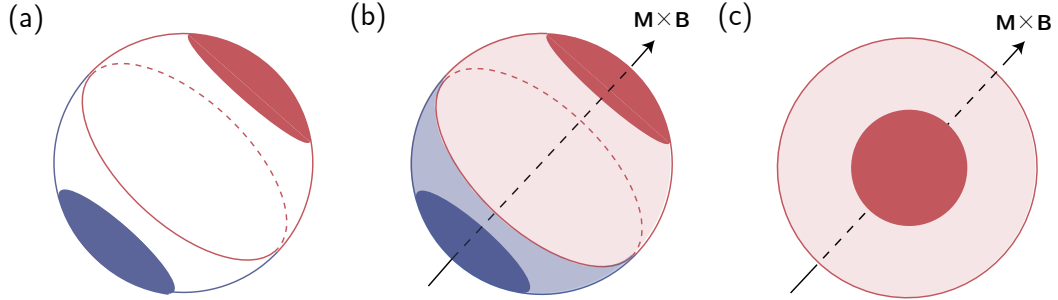


Figure S3. (a) Schematic of surface (pseudo)spin textures for non-closed case. Here the dark red and dark blue regions denote the textures of (pseudo)spins  $\mathbf{n}_{1(3)}$  and  $\mathbf{n}_{2(4)}$ , respectively. (b) The situation where  $\tilde{n}_{\text{WZ}}$  can be well-defined. Since the real surface (pseudo)spin texture regions are non-closed, we need to add the auxiliary textures (light red and light blue regions) to complement real regions and achieve a perfect unit sphere, which is dubbed “continuation”. And as long as the mass field vortex exists in real regions (the vector  $e_{\mathbf{M} \times \mathbf{B}}$  threads the dark color regions), we can obtain a nonzero two-particle WZ terms. (c) The situation where we can’t get a well-defined  $\tilde{n}_{\text{WZ}}$  since the mass field vortex locates in auxiliary regions.

$\{\mathbf{n}_3, \mathbf{n}_4\}_\beta$  with  $\mathbf{n}_1 = -\mathbf{n}_2 = \mathbf{n}_3 = -\mathbf{n}_4 = e_r$ . Correspondingly, the surface (pseudo)spin textures within  $S$  render two coincident unit spheres under the ideal condition. Thus we have

$$\begin{aligned}
 \tilde{n}_{\text{WZ}}^{(\alpha)} = \tilde{n}_{\text{WZ}}^{(\beta)} &= \frac{1}{4\pi} \left\{ \int_{\bar{S}_1} d\bar{\theta}_1 d\bar{\varphi}_1 [\mathbf{n}_1 \cdot (\partial_{\bar{\theta}_1} \mathbf{n}_1 \times \partial_{\bar{\varphi}_1} \mathbf{n}_1)] + \int_{\bar{S}_2} d\bar{\theta}_2 d\bar{\varphi}_2 [\mathbf{n}_2 \cdot (\partial_{\bar{\theta}_2} \mathbf{n}_2 \times \partial_{\bar{\varphi}_2} \mathbf{n}_2)] \right. \\
 &= \frac{1}{4\pi} \left\{ \int_{\bar{S}_3} d\bar{\theta}_3 d\bar{\varphi}_3 [\mathbf{n}_3 \cdot (\partial_{\bar{\theta}_3} \mathbf{n}_3 \times \partial_{\bar{\varphi}_3} \mathbf{n}_3)] + \int_{\bar{S}_4} d\bar{\theta}_4 d\bar{\varphi}_4 [\mathbf{n}_4 \cdot (\partial_{\bar{\theta}_4} \mathbf{n}_4 \times \partial_{\bar{\varphi}_4} \mathbf{n}_4)] \right. \\
 &= \frac{1}{4\pi} \int_{\text{sphere}} d\bar{\theta} d\bar{\varphi} [e_{\bar{r}} \cdot (\partial_{\bar{\theta}} e_{\bar{r}} \times \partial_{\bar{\varphi}} e_{\bar{r}})], \tag{S19}
 \end{aligned}$$

where  $\bar{\theta}_1 = \bar{\theta}_3, \bar{\theta}_2 = \bar{\theta}_4, \bar{\varphi}_1 = \bar{\varphi}_3, \bar{\varphi}_2 = \bar{\varphi}_4$ . For simplicity, we only take the  $\tilde{n}_{\text{WZ}}^{(\alpha)}$  as example to proceed the derivation, but the results are also the same with  $\tilde{n}_{\text{WZ}}^{(\beta)}$ . As shown in Fig.S2(c), Eq.(S19) can reduce to a line integral

$$\tilde{n}_{\text{WZ}}^{(\alpha)} = \tilde{n}_{\text{WZ}}^{(\beta)} = \frac{1}{2\pi} \oint_{\text{equator}} d\bar{\varphi} [\mathbf{e}_{\bar{z}} \cdot (\mathbf{e}_{\bar{r}}|_{\bar{\theta}=\frac{\pi}{2}} \times \partial_{\bar{\varphi}} \mathbf{e}_{\bar{r}}|_{\bar{\theta}=\frac{\pi}{2}})], \quad (\text{S20})$$

which indicates that the nonzero two-particle Wess-Zumino term ( $\tilde{n}_{\text{WZ}}^{(\alpha)} = \tilde{n}_{\text{WZ}}^{(\beta)} = 1$ ) can contribute to a nonzero winding numbers of surface normal vector  $\mathbf{e}_{\bar{r}}|_{\bar{\theta}=\frac{\pi}{2}}$  along the equator of unit sphere  $\bar{\mathbf{S}}_{1(3)} + \bar{\mathbf{S}}_{2(4)}$ . Transforming such integral from (pseudo)spin space to real space, the vector  $\mathbf{e}_{\bar{r}}|_{\bar{\theta}=\frac{\pi}{2}}$  is correspondingly mapped to vector  $\mathbf{e}_r$  on the boundary of  $\mathcal{S}$  [Fig.S2(d)]:

$$\begin{aligned} \tilde{n}_{\text{WZ}}^{(\alpha)} = \tilde{n}_{\text{WZ}}^{(\beta)} &= \frac{1}{2\pi} \oint_{\text{equator}} d\bar{\varphi} [\mathbf{e}_{\bar{z}} \cdot (\mathbf{e}_{\bar{r}}|_{\bar{\theta}=\frac{\pi}{2}} \times \partial_{\bar{\varphi}} \mathbf{e}_{\bar{r}}|_{\bar{\theta}=\frac{\pi}{2}})] = \frac{1}{2\pi} \oint_{\partial\mathcal{S}(\phi')} d\phi' [\mathbf{e}_{r=r_a} \cdot (\mathbf{e}_r \times \frac{\partial \bar{\varphi}}{\partial \phi'} \partial_{\bar{\varphi}} \mathbf{e}_r)] \\ &= \frac{1}{2\pi} \oint_{\partial\mathcal{S}(\phi')} d\phi' [\mathbf{e}_{r=r_a} \cdot (\mathbf{e}_r \times \partial_{\phi'} \mathbf{e}_r)]. \end{aligned} \quad (\text{S21})$$

Next, we discuss the connection between two-particle WZ term  $\tilde{n}_{\text{WZ}}$  and CS term  $\tilde{\theta}$ . According to (S-1), we can gap out the surface Dirac (Majorana) cone of total TIs (TSCs)  $\mathcal{H}_{\text{TI(TSC)}}^{\text{total}}$  and realize the TOTIs (TOTSCs) by applying a non-trivial surface effective mass field  $\mathbf{m} = (\mathbf{B}_\phi, \mathbf{M}_\phi)$ , and the surface effective Hamiltonian is usually given by  $\mathcal{H}_{\text{eff}} = -tk_\varphi \Gamma_1 + tk_\theta \Gamma_2 + \mathbf{B}_\phi \Gamma_3 + \mathbf{M}_\phi \Gamma_4$ . As a result, the Chern-Simons term  $\tilde{\theta}$  with respect to target corner  $\mathbf{a}$  is computed as  $\tilde{\theta} = \pi [\frac{1}{2\pi} \oint_{\partial\mathcal{S}(\phi)} d\phi \frac{\mathbf{M}_\phi \partial_\phi (\mathbf{B}_\phi) - \mathbf{B}_\phi \partial_\phi (\mathbf{M}_\phi)}{\mathbf{B}_\phi^2 + \mathbf{M}_\phi^2}]$ . Here the Dirac (Majorana) cone winding number has been taken as  $\mathcal{W}_h = 1$ , and  $\partial\mathcal{S}$  represents the boundary of area  $\mathcal{S}$ . As sketched in Fig.S2(e) and (f), we consider a kind of specialized surface mass field  $(\mathbf{B}_\phi, \mathbf{M}_\phi) = (\mathbf{e}_r \cdot \mathbf{B}, \mathbf{e}_r \cdot \mathbf{M})$  with  $\mathbf{B}$  and  $\mathbf{M}$  been constant unit vectors, thus the Chern-Simons term  $\tilde{\theta}$  becomes

$$\tilde{\theta} = \pi \left\{ \frac{1}{2\pi} \oint_{\partial\mathcal{S}(\phi)} d\phi \left[ \frac{(\mathbf{e}_r \cdot \mathbf{M})(\partial_\phi \mathbf{e}_r \cdot \mathbf{B}) - (\mathbf{e}_r \cdot \mathbf{B})(\partial_\phi \mathbf{e}_r \cdot \mathbf{M})}{(\mathbf{e}_r \cdot \mathbf{B})^2 + (\mathbf{e}_r \cdot \mathbf{M})^2} \right] \right\} = \frac{1}{2} \oint_{\partial\mathcal{S}(\phi)} d\phi [\mathbf{e}_{\mathbf{M} \times \mathbf{B}} \cdot (\mathbf{e}_r \times \partial_\phi \mathbf{e}_r)] \frac{|\mathbf{M} \times \mathbf{B}|}{\mathbf{B}_\phi^2 + \mathbf{M}_\phi^2} \quad (\text{S22})$$

As we can see, the two-particle WZ term  $\tilde{n}_{\text{WZ}}$  in Eq.(S21) is closely related to Chern-Simons term  $\tilde{\theta}$  in Eq.(S22). When  $|\mathbf{e}_{r=r_a} \cdot \mathbf{e}_{\mathbf{M} \times \mathbf{B}}| = 1$  and  $\mathbf{M} \perp \mathbf{B}$ , we have  $|\tilde{\theta}| = \pi |\tilde{n}_{\text{WZ}}^{(\alpha)}| = \pi |\tilde{n}_{\text{WZ}}^{(\beta)}|$ . Notice that this equality is also applied to a more general case:  $|\mathbf{e}_{r=r_a} \cdot \mathbf{e}_{\mathbf{M} \times \mathbf{B}}| \leq 1$  and  $\mathbf{M} \nparallel \mathbf{B}$ . This result reflects that the two-particle WZ terms  $\tilde{n}_{\text{WZ}}$  can render a nonzero Chern-Simons term  $\tilde{\theta}$  under the specialized effective mass field  $(\mathbf{e}_r \cdot \mathbf{B}, \mathbf{e}_r \cdot \mathbf{M})$ . Namely, we can predict the existence of zero corner modes of TOTIs (TOTSCs) in terms of  $\tilde{n}_{\text{WZ}}$  which is derived from the surface (pseudo)spin textures around target corner.

However, as shown in [Fig.S3(a)], the surface (pseudo)spin textures defined on  $\mathcal{S}$  are usually not closed (dark red and dark blue spherical crowns). Are the conclusions above still valid? The answer is yes. To demonstrate this we will resort to the method: ‘‘continuation’’, which means the auxiliary (pseudo)spin textures [light red and light blue regions in Fig.S3(b)] are added to complement the real (pseudo)spin textures, rendering a perfect unit sphere. Remarkably, the surface effective mass nodes must be guaranteed to locate in real (pseudo)spin texture regions. With this method, the two-particle WZ terms  $\tilde{n}_{\text{WZ}}$  can be well-defined. For example, as plotted in [Fig.S3(b)],  $\mathbf{e}_{\mathbf{M} \times \mathbf{B}}$  pierces the dark red and dark blue actual (pseudo)spin texture regions, making the effective mass field vortex exist in them. Thus we have  $\tilde{n}_{\text{WZ}}^\alpha = \tilde{n}_{\text{WZ}}^\beta = 1$  after ‘‘continuation’’. In contrast, the two-particle WZ term can't be well-defined and disappear for the case shown in [Fig.S3(c)]. In conclusion, the two-particle WZ  $\tilde{n}_{\text{WZ}}$  term mechanism can be stated as follow: if the non-trivial (pseudo)spin textures around target corner support the nonzero  $\tilde{n}_{\text{WZ}}$ , a zero energy bound state localizes at the corner with specialized surface mass field  $(\mathbf{e}_r \cdot \mathbf{B}, \mathbf{e}_r \cdot \mathbf{M})$  applied.

### S-3. FEASIBLE PHYSICAL REALIZATIONS FOR TOTIS (TOTSCS)

The surface Chern-Simons theory ( $\tilde{\theta}$  characterization and  $\tilde{n}_{\text{WZ}}$  mechanism) provides a generic and intuitive 2D effective surface theoretical description for the emergence of zero energy corner modes of TOTIs (TOTSCs), which opens a new avenue toward the realizations of TOTIs and TOTSCs and guides us to search for the underlying material candidates. In the following, we provide the feasible physical realization schemes respectively for TOTIs and TOTSCs.

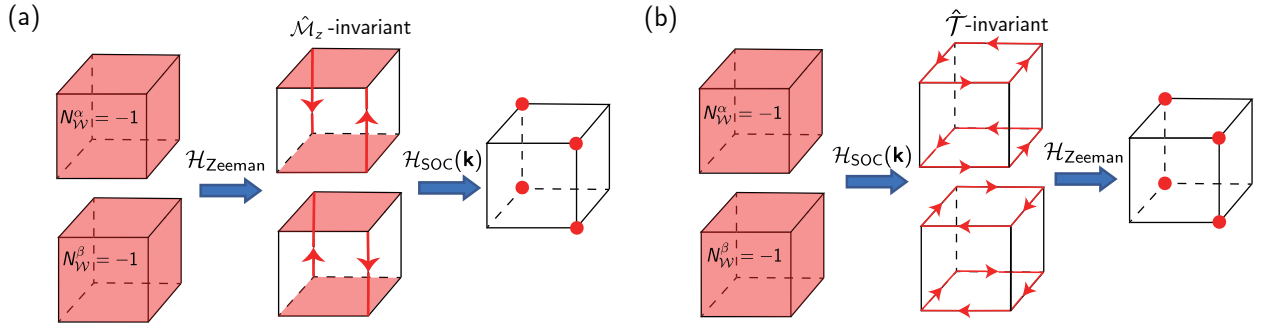


Figure S4. Symmetry analysis for Majorana zero corner modes of TOTSCs. (a) The total TSC is constructed by stacking two copies of minimal  $\mathcal{T}$ -invariant TSCs. Applying an in-plane Zeeman field produces the helical hinge modes protected by  $\mathcal{M}_z$  symmetry. Then SOC term opens gap and introduces mass-inversion between adjacent hinges, leading to Majorana zero corner modes. (b) Alternatively, adding SOC term breaks  $\mathcal{M}_z$  symmetry while keeps  $\mathcal{T}$  symmetry, thus a pair of helical hinge modes protected by  $\mathcal{T}$  appear. Then an in-plane Zeeman term lifts  $\mathcal{T}$  symmetry and gives rise to Majorana zero corner modes.

## A. Realization scheme for TOTSCs

### 1. $\tilde{\theta}$ characterization

Let us start from the Hamiltonian for TOTSCs:

$$\mathcal{H}_{\text{TOTSC}}(\mathbf{k}) = \mathcal{H}_{\text{TSC}}^{\text{total}}(\mathbf{k}) + \mathcal{H}_{\text{Zeeman}} + \mathcal{H}_{\text{SOC}}(\mathbf{k}). \quad (\text{S23})$$

The 3D total TSC, which is constructed by stacking two copies of minimal 3D TSCs:  $\mathcal{H}_{\text{TSC}}^{\text{total}}(\mathbf{k}) = \mathcal{H}_{\text{TSC}}^{\alpha}(\mathbf{k}) \oplus \mathcal{H}_{\text{TSC}}^{\beta}(\mathbf{k})$ , is described by Hamiltonian:  $\mathcal{H}_{\text{TSC}}^{\text{total}}(\mathbf{k}) = \frac{\Delta_p}{k_F} \sum_{j=x,y} \sin k_j \sigma_0 \tau_x s_j + \frac{\Delta_p}{k_F} \sin k_z \sigma_z \tau_x s_z - (\mu - \frac{3}{m_*} + \frac{1}{m_*} \sum_{j=x,y,z} \cos k_j) \sigma_z \tau_z s_0$ , where  $\{\sigma\}$ ,  $\{\tau\}$  and  $\{s\}$  represent the Pauli matrices acting on orbital, Nambu and spin space, respectively. Furthermore, the Zeeman term reads  $\mathcal{H}_{\text{Zeeman}} = \mathbf{B}_{\parallel} \cdot \mathbf{s}$  with  $\mathbf{B}_{\parallel} = (\frac{\sqrt{2}}{2}, \frac{\sqrt{2}}{2}, 0)$  and the spin-orbit coupling (SOC) term  $\mathcal{H}_{\text{SOC}}(\mathbf{k})$  keeps the time-reversal symmetry  $\hat{\mathcal{T}} = -i s_y \kappa$  since  $\hat{\mathcal{T}}^{-1} \mathcal{H}_{\text{SOC}}(\mathbf{k}) \hat{\mathcal{T}} = \hat{\mathcal{T}}^{-1} [-\lambda_{so,0} + \lambda_{so,1} (\cos k_x + \cos k_y)] \sigma_y s_z \hat{\mathcal{T}} = \mathcal{H}_{\text{SOC}}(-\mathbf{k})$ . Now we use  $\tilde{\theta}$  characterization to identify the 3rd-order zero energy corner modes. We solve the topological surface states from  $\mathcal{H}_{\text{TSC}}^{\text{total}}(\mathbf{k})$  for surface  $\Sigma(\theta = \frac{\pi}{2}, \phi)$  in cylindrical coordinate system:

$$\begin{aligned} |\epsilon_1\rangle &= \frac{1}{2} \begin{pmatrix} 1 \\ 0 \end{pmatrix}_{\sigma} \otimes \begin{pmatrix} 1 \\ i \end{pmatrix}_{\tau} \otimes \begin{pmatrix} 1 \\ +e^{i\phi} \end{pmatrix}_s; & |\epsilon_2\rangle &= \frac{1}{2} \begin{pmatrix} 1 \\ 0 \end{pmatrix}_{\sigma} \otimes \begin{pmatrix} 1 \\ -i \end{pmatrix}_{\tau} \otimes \begin{pmatrix} 1 \\ -e^{i\phi} \end{pmatrix}_s \\ |\epsilon_3\rangle &= \frac{1}{2} \begin{pmatrix} 0 \\ 1 \end{pmatrix}_{\sigma} \otimes \begin{pmatrix} 1 \\ i \end{pmatrix}_{\tau} \otimes \begin{pmatrix} 1 \\ -e^{i\phi} \end{pmatrix}_s; & |\epsilon_4\rangle &= \frac{1}{2} \begin{pmatrix} 0 \\ 1 \end{pmatrix}_{\sigma} \otimes \begin{pmatrix} 1 \\ -i \end{pmatrix}_{\tau} \otimes \begin{pmatrix} 1 \\ +e^{i\phi} \end{pmatrix}_s, \end{aligned} \quad (\text{S24})$$

where  $\phi$  is the azimuthal angle. And we can readily obtain the effective surface Hamiltonian  $\mathcal{H}_{\text{effective}} = t_p k_{\phi} \tilde{\sigma}_z \tilde{\tau}_x + t_p k_z \tilde{\sigma}_z \tilde{\tau}_y + m_{\phi} \tilde{\sigma}_z \tilde{\tau}_z + m_{\theta} \tilde{\sigma}_y \tilde{\tau}_0$  with effective velocity  $t_p = \frac{\Delta_p}{k_F}$ . Since magnetic field  $\mathbf{B}_{\parallel} = (\frac{\sqrt{2}}{2}, \frac{\sqrt{2}}{2}, 0)$  is deposited on the  $x - y$  plane, the resulting effective mass  $m_{\phi} = \mathbf{B}_{\parallel} \cdot \mathbf{e}_{\rho}$  forms a domain wall spreading along the meridian  $\mathbf{l}_{\phi=3\pi/4}$ . Moreover, the effective mass  $m_{\theta}$  generated by  $\mathcal{H}_{\text{SOC}}(\mathbf{k})$  is dependent on  $\theta$  ( $m_{\theta} = -\lambda_{so,0} + 2\lambda_{so,1} - \lambda_{so,1} \frac{4\mu - \frac{m_*^2}{4} - 1}{2} \sin^2 \theta$ ) and its mass domain walls are present at two parallels  $\mathbf{l}_{\theta_1}$  and  $\mathbf{l}_{\theta_2}$ . Then we can get four intersections of  $\mathbf{l}_{\phi=3\pi/4}$  and  $\mathbf{l}_{\theta_1}, \mathbf{l}_{\theta_2}$ , which serve as the vortices of surface mass field ( $m_{\phi}, m_{\theta}$ ) here and contribute to the nonzero mass field winding numbers. Notice that the surface Majorana cone winding number has been taken as  $\mathcal{W}_h = 1$ . As a result, there are totally four zero energy bound states at the intersections according to  $\tilde{\theta}$  characterization, which means the TOTSCs dictated by Eq.(S23) features four Majorana zero corner modes. The numerical results displayed in Fig.3(d) of main text confirm this prediction.

### 2. Symmetry analysis

Finally, we show that the existence of Majorana zero corner modes can also be deduced from symmetry analysis. It's known that the 3D total TSC preserves time-reversal symmetry as  $\hat{\mathcal{T}}^{-1} \mathcal{H}_{\text{TSC}}^{\text{total}}(\mathbf{k}) \hat{\mathcal{T}} = \mathcal{H}_{\text{TSC}}^{\text{total}}(-\mathbf{k})$ . Adding in-plane magnetic field  $\mathbf{B}_{\parallel}$ ,  $\hat{\mathcal{T}}$  symmetry is broken and a pair of helical hinge states which result from the sign-inversion of  $\mathbf{B}_{\phi} = \mathbf{B} \cdot \mathbf{e}_{\rho}$  propagate

along  $z$  direction. Notice that mirror symmetry  $\hat{M}_z = \sigma_x \tau_x$  can relate helical hinge modes since BdG Hamiltonian  $\mathcal{H}_{\text{BdG}}(\mathbf{k}) = \mathcal{H}_{\text{TSC}}^{\text{total}}(\mathbf{k}) + \mathcal{H}_{\text{Zeeman}}$  is  $\hat{M}_z$  invariant:  $\hat{M}_z^{-1} \mathcal{H}_{\text{BdG}}(k_x, k_y, k_z) \hat{M}_z = \mathcal{H}_{\text{BdG}}(k_x, k_y, -k_z)$ . In other words, these gapless hinge modes are protected by  $\hat{M}_z$ . In addition, since  $\mathcal{H}_{\text{BdG}}(\mathbf{k})$  is  $\sigma_z$ -conserved, the two species of helical hinge modes correspond to eigenvalues  $\sigma_z = +1$  and  $\sigma_z = -1$ , respectively. Thus, we can consider a  $\sigma_z$ -non-conserved term  $\mathcal{H}_{\text{SOC}}(\mathbf{k})$  which couples the helical hinge modes by breaking  $\hat{M}_z$  symmetry and changes sign between adjacent hinges to induce Majorana zero corner modes. The schematic diagram is plotted in Fig.S4(a).

Alternatively, exchanging the order of application of  $\mathcal{H}_{\text{Zeeman}}$  and  $\mathcal{H}_{\text{SOC}}(\mathbf{k})$  still achieve the same result [Fig.S4(b)]. The  $\hat{M}_z$  symmetry is broken with  $\mathcal{H}_{\text{SOC}}(\mathbf{k})$  introduced while  $\hat{T}$  symmetry also retains since  $\hat{T}^{-1} \mathcal{H}'_{\text{BdG}}(\mathbf{k}) \hat{T} = \hat{T}^{-1} [\mathcal{H}_{\text{TSC}}^{\text{total}}(\mathbf{k}) + \mathcal{H}_{\text{SOC}}(\mathbf{k})] \hat{T} = \mathcal{H}'_{\text{BdG}}(-\mathbf{k})$ . And the sign-changing of  $M_\phi$  enforces two pairs of helical hinge modes which are protected by  $\hat{T}$ . Thus we can gap out the gapless hinge modes by considering  $\hat{T}$ -breaking Zeeman term  $\mathcal{H}_{\text{Zeeman}}$ , leading to Majorana zero corner modes. We emphasize that the conclusion based on symmetry analysis is consistent with that from  $\hat{\theta}$  characterization.

### 3. Physical realization

In this subsection, we provide some physical details for the feasible realization scheme of  $\mathcal{H}_{\text{TOTSC}}(\mathbf{k})$ . Obviously, Zeeman term  $\mathcal{H}_{\text{Zeeman}} = \mathbf{B}_{\parallel} \cdot \mathbf{s}$  can be achieved by applying an in-plane magnetic field to the 3D total TSC. For the time-reversal invariant SOC  $\mathcal{H}_{\text{SOC}}(\mathbf{k})$ , we can realize this term in a multi-orbital square lattice [Fig.3(a) in main text] with two orbitals  $\{\alpha, \beta\}$  within a site. And we find the corresponding SOC term in real space takes the form of

$$\hat{H}_{\text{SOC}}^{\text{I}} = \sum_i -i\lambda_{so,0} (\hat{C}_{i,\alpha}^\dagger s_z \hat{C}_{i,\beta} - \hat{C}_{i,\beta}^\dagger s_z \hat{C}_{i,\alpha}) + \sum_{\langle i,j \rangle} \left( \frac{i\lambda_{so,1}}{2} \hat{C}_{i,\alpha}^\dagger s_z \hat{C}_{j,\beta} + \text{h.c.} \right), \quad (\text{S25})$$

where  $\hat{c}_{i,\alpha(\beta)}^\dagger = (c_{i,\alpha(\beta),\uparrow}^\dagger, c_{i,\alpha(\beta),\downarrow}^\dagger)$  and  $\hat{c}_{i,\alpha(\beta)} = (c_{i,\alpha(\beta),\uparrow}, c_{i,\alpha(\beta),\downarrow})$  represent the creation and annihilation operators, respectively. Here we emphasize that the time-reversal invariant  $\hat{H}_{\text{SOC}}^{\text{I}}$  involves two parts: the on-site term (the former) and the nearest-neighbour term (the latter) [Fig.3(b) in main text] with  $\lambda_{so,0}, \lambda_{so,1}$  denoting the corresponding SOC strengths. Notably, these orbitals  $\{\alpha, \beta\}$  can be chosen as  $(p_x, p_y), (d_{xz}, d_{yz}), (d_{xy}, d_{x^2-y^2})$ . Remarkly, the realistic superconducting system  $\beta$ -PdBi<sub>2</sub> which exhibits  $p$ -wave pairing and topological surface states meets this condition since the maximal contributions to its density of states at the Fermi level come from Bi  $6p_{x+y}$  orbitals, indicating that it may serve as a potential candidate.

## B. Realization scheme for TOTIs

The proposal for TOTIs exploits the stagger Zeeman term and SOC term with model Hamiltonian given by

$$\mathcal{H}_{\text{TOTIs}}(\mathbf{k}) = \mathcal{H}_{\text{TI}}^{\text{total}}(\mathbf{k}) + \mathcal{H}_{\text{s-Zeeman}} + \mathcal{H}_{\text{SOC}}. \quad (\text{S26})$$

The Hamiltonian for total 3D TI ( $\mathcal{H}_{\text{TI}}^a \oplus \mathcal{H}_{\text{TI}}^b$ ) reads  $\mathcal{H}_{\text{TI}}^{\text{total}}(\mathbf{k}) = (m - t \sum_i \cos k_i) \rho_0 s_0 \sigma_z + t (\sum_i \sin k_i \rho_0 s_i) \sigma_x$ , where  $\{\rho\}, \{\sigma\}$  and  $\{s\}$  are Pauli matrices in sublattice, orbital and spin space, respectively. In addition, the stagger Zeeman term reads  $\mathcal{H}_{\text{s-Zeeman}} = \rho_z \mathbf{B}_{\parallel} \cdot \mathbf{s}$  and SOC term considered here still keeps time-reversal symmetry as  $\hat{T}^{-1} \mathcal{H}_{\text{SOC}} \hat{T} = \hat{T}^{-1} (\rho_y \mathbf{M} \cdot \mathbf{s}) \hat{T} = \hat{T}^{-1} (\lambda_{so} \rho_y s_z) \hat{T} = \lambda_{so} \rho_y s_z = \mathcal{H}_{\text{SOC}}$ .

### 1. $\tilde{n}_{\text{WZ}}$ mechanism

We first solve the topological surface states on surface  $\Sigma(\theta, \varphi)$ :

$$\begin{aligned} |\varepsilon_1\rangle &= \begin{pmatrix} 1 \\ 0 \end{pmatrix}_\rho \otimes \frac{1}{\sqrt{2}} \begin{pmatrix} 1 \\ -i \end{pmatrix}_\sigma \otimes \begin{pmatrix} \cos \theta/2 \\ e^{i\phi} \sin \theta/2 \end{pmatrix}_s; & |\varepsilon_2\rangle &= \begin{pmatrix} 1 \\ 0 \end{pmatrix}_\rho \otimes \frac{1}{\sqrt{2}} \begin{pmatrix} 1 \\ i \end{pmatrix}_\sigma \otimes \begin{pmatrix} \sin \theta/2 \\ -e^{i\phi} \cos \theta/2 \end{pmatrix}_s \\ |\varepsilon_3\rangle &= \begin{pmatrix} 0 \\ 1 \end{pmatrix}_\rho \otimes \frac{1}{\sqrt{2}} \begin{pmatrix} 1 \\ -i \end{pmatrix}_\sigma \otimes \begin{pmatrix} \cos \theta/2 \\ e^{i\phi} \sin \theta/2 \end{pmatrix}_s; & |\varepsilon_4\rangle &= \begin{pmatrix} 0 \\ 1 \end{pmatrix}_\rho \otimes \frac{1}{\sqrt{2}} \begin{pmatrix} 1 \\ i \end{pmatrix}_\sigma \otimes \begin{pmatrix} \sin \theta/2 \\ -e^{i\phi} \cos \theta/2 \end{pmatrix}_s. \end{aligned} \quad (\text{S27})$$

Projecting the two constant terms  $(\rho_z \mathbf{B}_{\parallel} \cdot \mathbf{s}, \rho_y \mathbf{M} \cdot \mathbf{s})$  onto surface states subspace yields a specialized surface mass field  $(\mathbf{e}_r \cdot \mathbf{B}_{\parallel}, \mathbf{e}_r \cdot \mathbf{M})$ . The (pseudo)spin polarizations are  $\{\mathbf{n}_1, \mathbf{n}_2\}_a$  and  $\{\mathbf{n}_3, \mathbf{n}_4\}_b$  where  $\mathbf{n}_i = \langle \varepsilon_i | \mathbf{s} | \varepsilon_i \rangle$  with  $\mathbf{n}_1 = -\mathbf{n}_2 = \mathbf{n}_3 = -\mathbf{n}_4 = \mathbf{e}_r$ . As shown in Fig.S5(a), we focus on a regular octahedron sample and take target corner  $\mathbf{c}$  as an example to predict the

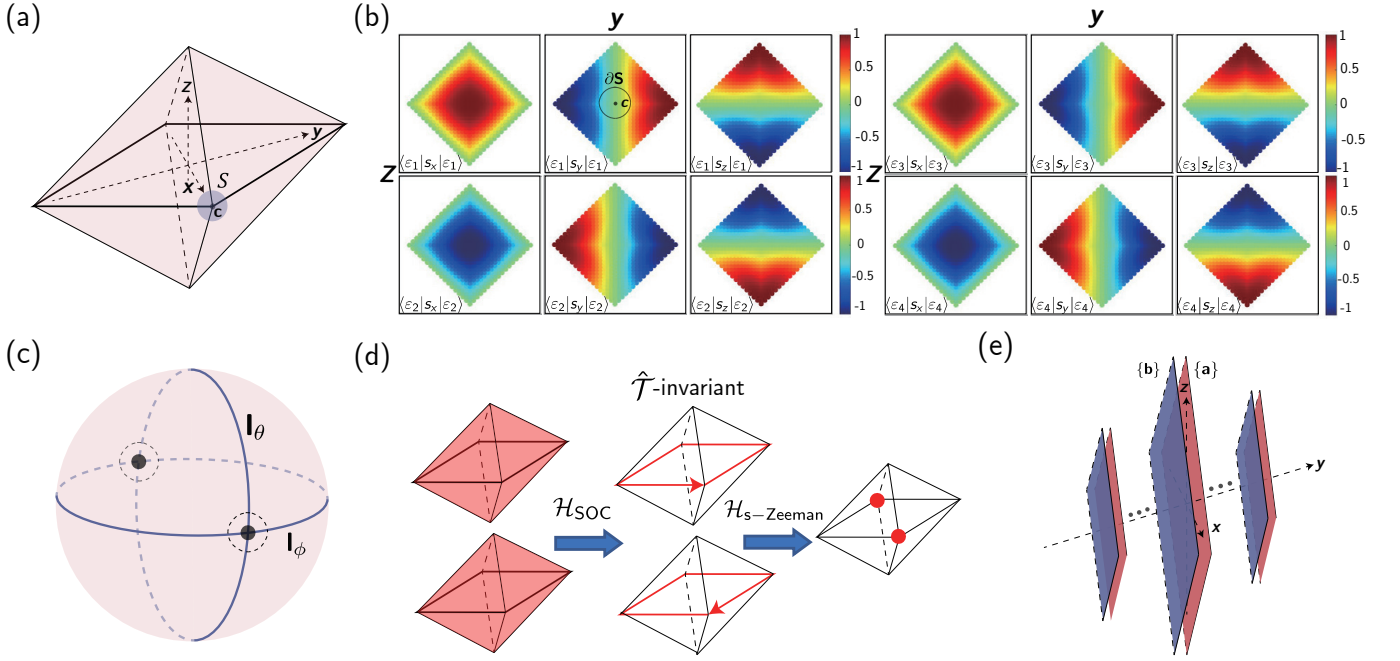


Figure S5. (a) The sample geometry. We consider a regular octahedron here and focus on an area  $\mathcal{S}$  centered at corner  $c$ . (b) The distributions of surface (pseudo)spins ( $\mathbf{n}_1, \mathbf{n}_2, \mathbf{n}_3, \mathbf{n}_4$ ) expectations on the  $y - z$  plane. The black circle denotes  $\partial\mathcal{S}$  and  $c$  is target corner. (c)  $\hat{\theta}$  characterization for TOTIs.  $\mathbf{l}_\phi$  and  $\mathbf{l}_\theta$  represent the mass domain walls generated by  $\mathcal{H}_{\text{SOC}}$  and  $\mathcal{H}_{\text{s-Zeeman}}$ , respectively. The black dots, which are intersections of  $\mathbf{l}_\phi$  and  $\mathbf{l}_\theta$ , stand for surface mass field vortices and contribute to nonzero winding numbers. (d) Symmetry analysis for the emergence of zero corner modes. (e) The arrangement of sublattice layers  $\{a\}$  and  $\{b\}$ .

emergence of zero corner modes in terms of  $\tilde{n}_{\text{WZ}}$  mechanism. Now let's consider an area  $\mathcal{S}$  and study the surface (pseudo)spin textures on it. As we can see, these textures [Fig.S5(b) and Fig.S4(c)] can't constitute the perfect unit spheres, so we need "continuation" [Fig.4(c) in main text] to complement the real (pseudo)spin textures. Moreover, we find  $e_{\mathbf{M} \times \mathbf{B}_\parallel} = e_{r=r_c}(e_x)$  since  $\mathbf{B}_\parallel = (0, -1, 0)$  and  $\mathbf{M} = (0, 0, 1)$ . Therefore, we can get  $\tilde{n}_{\text{WZ}}^a = \tilde{n}_{\text{WZ}}^b = 1$  and predict the existence of zero corner mode with  $(\rho_z \mathbf{B}_\parallel \cdot \mathbf{s}, \rho_y \mathbf{M} \cdot \mathbf{s})$  introduced. This TOTI totally supports two zero corner modes and numerical results shown in Fig.4(d) in main text favor such conclusions.

## 2. Symmetry analysis

The symmetry analysis can also guide us to identify zero corner mode. As shown in Fig.S5(d), the 3D total TI  $\mathcal{H}_{\text{TI}}^{\text{total}}$  involves two copies of minimal TIs  $\mathcal{H}_{\text{TI}}^a(\mathbf{k})$  and  $\mathcal{H}_{\text{TI}}^b(\mathbf{k})$  which are characterized by the same  $\mathbb{Z}_2$  index ( $\mathbb{Z}_2 = 1$ ). Thus the surface Dirac cones of total TI can be gapped out by effective mass  $\tilde{M}_\phi$  derived from time-reversal invariant SOC term  $\mathcal{H}_{\text{SOC}} = \rho_y \mathbf{M} \cdot \mathbf{s}$  and the sign-inversion of  $\tilde{M}_\phi$  between adjacent surfaces leads to helical hinge modes protected by  $\hat{T}$ -symmetry. In order to obtain the zero corner modes,  $\hat{T}$ -breaking in-plane staggered Zeeman field  $\mathcal{H}_{\text{s-Zeeman}} = \rho_z \mathbf{B}_\parallel \cdot \mathbf{s}$  is necessary. Notice that the Hamiltonian  $\mathcal{H}_{\text{TOTIs}}(\mathbf{k})$  considered here does not maintain inversion symmetry  $\hat{I} = \rho_z \sigma_z$  since  $\hat{I}^{-1} \mathcal{H}_{\text{TOTIs}}(\mathbf{k}) \hat{I} \neq \mathcal{H}_{\text{TOTIs}}(-\mathbf{k})$ , which agrees with the classification theory proposed in [7].

## 3. Physical realization

As displayed in Fig.S5(e), the bipartite square lattices are adopted and  $(a, b)$  denote two different sublattice sites within a unit cell. Moreover, the 2D layers  $\{a\}$  and  $\{b\}$  are parallel to  $x - y$  plane and arranged alternatively along  $y$ -axis. Therefore, the staggered Zeeman term  $\mathcal{H}_{\text{s-Zeeman}} = \rho_z \mathbf{B}_\parallel \cdot \mathbf{s}$  with  $\mathbf{B}_\parallel = (0, -1, 0)$  can be achieved by applying antiferromagnetism between layer  $\{a\}$  and  $\{b\}$ . For  $\hat{T}$ -invariant SOC term considered here, we find it only remains the real space intra-cell term

$$\hat{H}_{\text{SOC}}^{\text{II}} = \sum_i -i\lambda_{\text{so}} (\hat{C}_{i,a}^\dagger s_z \hat{C}_{i,b} - \hat{C}_{i,b}^\dagger s_z \hat{C}_{i,a}). \quad (\text{S28})$$

In the following, we take the 3D bulk  $\text{MnBi}_2\text{Te}_4$  which is predicted as the antiferromagnetic (AFM) TI as a example to demonstrate the realization of TOTI phase.  $\text{MnBi}_2\text{Te}_4$  is a tetradymite compound consisting of stacked Te-Bi-Te-Mn-Te-Bi-Te septuple layers (SLs). And the spins of Mn exhibit the intralayer ferromagnetism (within a single SL) and interlayer antiferromagnetism (between neighbouring SLs). Here we consider the sample geometry shown in Fig.S5(a) and AFM orders along  $y$ -direction. The staggered Zeeman term  $\mathcal{H}_{s\text{-Zeeman}}$  can be provided by the interlayer antiferromagnetism. Thus, a pair of helical edge states emerge at corresponding hinges. In addition, the  $\hat{T}$ -invariant SOC term  $\hat{H}_{\text{SOC}}^{\text{II}}$  is promising to be realized by introduce the spin-dependent couplings between Mn atoms of neighbouring SLs, which couples the helical edge states and contributes a sign-inversion mass of adjacent hinges. As a result, we can obtain the 3rd-order corner modes. According to the above discussion, we conjecture that the 3D AFM TI  $\text{MnBi}_2\text{Te}_4$  may be a ideal platform to realize the TOTIs.

---

\* Corresponding author: xiongjunliu@pku.edu.cn.

- [1] C.-K. Chiu, J. C. Y. Teo, A. P. Schnyder, and S. Ryu, Classification of topological quantum matter with symmetries, *Rev. Mod. Phys.* **88**, 035005 (2016).
- [2] C. Chan, L. Zhang, T. F. J. Poon, Y.-P. He, Y.-Q. Wang, and X.-J. Liu, Generic Theory for Majorana Zero Modes in 2D Superconductors, *Phys. Rev. Lett.* **119**, 047001 (2017).
- [3] W. A. Benalcazar, B. A. Bernevig, and T. L. Hughes, Quantized electric multipole insulators, *Science* **357**, 61 (2017).
- [4] W. A. Benalcazar, B. A. Bernevig, and T. L. Hughes, Electric multipole moments, topological multipole moment pumping, and chiral hinge states in crystalline insulators, *Phys. Rev. B* **96**, 245115 (2017).
- [5] Y. Tan, Z.-H. Huang, and X.-J. Liu, Two-particle Berry phase mechanism for Dirac and Majorana Kramers pairs of corner modes, *Phys. Rev. B* **105**, L041105 (2022).
- [6] E. Khalaf, H. C. Po, A. Vishwanath, and H. Watanabe, Symmetry Indicators and Anomalous Surface States of Topological Crystalline Insulators, *Phys. Rev. X* **8**, 031070 (2018).
- [7] E. Khalaf, Higher-order topological insulators and superconductors protected by inversion symmetry, *Phys. Rev. B* **97**, 205136 (2018).
- [8] N. Bultinck, B. A. Bernevig, and M. P. Zaletel, Three-dimensional superconductors with hybrid higher-order topology, *Phys. Rev. B* **99**, 125149 (2019)